



# A high-resolution time-of-flight chemical ionization mass spectrometer utilizing hydronium ions ( $\text{H}_3\text{O}^+$ ToF-CIMS) for measurements of volatile organic compounds in the atmosphere

Bin Yuan<sup>1,2</sup>, Abigail Koss<sup>1,2,3</sup>, Carsten Warneke<sup>1,2</sup>, Jessica B. Gilman<sup>1</sup>, Brian M. Lerner<sup>1,2</sup>, Harald Stark<sup>2,3,4</sup>, and Joost A. de Gouw<sup>1,2,3</sup>

<sup>1</sup>NOAA Earth System Research Laboratory (ESRL), Chemical Sciences Division, Boulder, CO, USA

<sup>2</sup>Cooperative Institute for Research in Environmental Sciences, University of Colorado at Boulder, Boulder, CO, USA

<sup>3</sup>Department of Chemistry and Biochemistry, University of Colorado at Boulder, CO, USA

<sup>4</sup>Aerodyne Research Inc., Billerica, MA 01821, USA

Correspondence to: Bin Yuan (bin.yuan@noaa.gov)

Received: 20 January 2016 – Published in Atmos. Meas. Tech. Discuss.: 9 February 2016

Revised: 17 May 2016 – Accepted: 9 June 2016 – Published: 1 July 2016

**Abstract.** Proton transfer reactions between hydronium ions ( $\text{H}_3\text{O}^+$ ) and volatile organic compounds (VOCs) provide a fast and highly sensitive technique for VOC measurements, leading to extensive use of proton-transfer-reaction mass spectrometry (PTR-MS) in atmospheric research. Based on the same ionization approach, we describe the development of a high-resolution time-of-flight chemical ionization mass spectrometer (ToF-CIMS) utilizing  $\text{H}_3\text{O}^+$  as the reagent ion. The new  $\text{H}_3\text{O}^+$  ToF-CIMS has sensitivities of 100–1000 cps ppb<sup>-1</sup> (ion counts per second per part-per-billion mixing ratio of VOC) and detection limits of 20–600 ppt at  $3\sigma$  for a 1 s integration time for simultaneous measurements of many VOC species of atmospheric relevance. The ToF analyzer with mass resolution ( $m/\Delta m$ ) of up to 6000 allows the separation of isobaric masses, as shown in previous studies using similar ToF-MS. While radio frequency (RF)-only quadrupole ion guides provide better overall ion transmission than ion lens system, low-mass cutoff of RF-only quadrupole causes  $\text{H}_3\text{O}^+$  ions to be transmitted less efficiently than heavier masses, which leads to unusual humidity dependence of reagent ions and difficulty obtaining a humidity-independent parameter for normalization. The humidity dependence of the instrument was characterized for various VOC species and the behaviors for different species can be explained by compound-specific properties that affect the ion chemistry (e.g., proton affinity and dipole moment). The new  $\text{H}_3\text{O}^+$  ToF-CIMS was successfully deployed on the NOAA WP-3D

research aircraft for the SONGNEX campaign in spring of 2015. The measured mixing ratios of several aromatics from the  $\text{H}_3\text{O}^+$  ToF-CIMS agreed within  $\pm 10\%$  with independent gas chromatography measurements from whole air samples. Initial results from the SONGNEX measurements demonstrate that the  $\text{H}_3\text{O}^+$  ToF-CIMS data set will be valuable for the identification and characterization of emissions from various sources, investigation of secondary formation of many photochemical organic products and therefore the chemical evolution of gas-phase organic carbon in the atmosphere.

## 1 Introduction

Volatile organic compounds (VOCs) are ubiquitous in the atmosphere. The oxidation of VOCs contributes to formation of ozone (Atkinson, 2000) and secondary organic aerosol (SOA) (Hallquist et al., 2009). Accurate measurements of VOCs in the atmosphere are essential to understanding their sources, chemical transformations and hence their effects on ozone and SOA formation (Isaksen et al., 2009). Measurements of VOCs require techniques with high time resolution to effectively capture their high variability in the atmosphere, especially for measurements performed on mobile platforms.

Proton-transfer-reaction mass spectrometry (PTR-MS) has been an important scientific tool for VOC measurements, associated with high sensitivity and fast time response

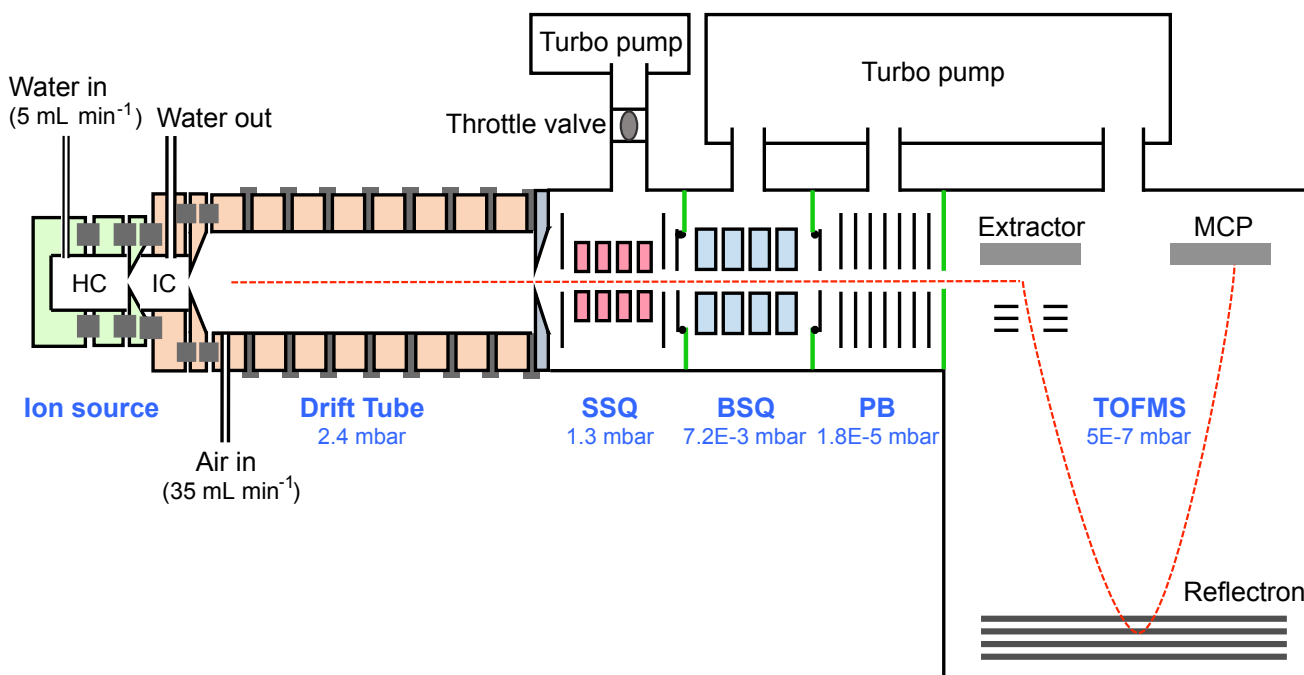


**Figure 1.** Schematic drawing of the  $\text{H}_3\text{O}^+$  ToF-CIMS. HC: hollow-cathode discharge; IC: intermediate chamber; SSQ: small segmented quadrupole; BSQ: big segmented quadrupole; PB: primary beam; MCP: microchannel plate detector.

(Lindinger et al., 1998; de Gouw and Warneke, 2007; Blake et al., 2009). Early PTR-MS instruments used a quadrupole mass spectrometer (QMS) for ion detection. PTR-QMS instruments usually step through several pre-selected masses consecutively each with a dwell time of 0.1–1 s (Warneke et al., 2015). The time resolution of PTR-QMS is generally sufficient for ground-based measurements targeting VOC mixing ratios but not ideal for aircraft measurements or eddy covariance flux measurements of more than a few species. Other mass analyzers, e.g., ion traps (Warneke et al., 2005; Steeghs et al., 2007; Mielke et al., 2008) and time-of-flight (ToF) mass spectrometers (Blake et al., 2004; Ennis et al., 2005; Tanimoto et al., 2007), have been used to overcome some of these inherent drawbacks in PTR-QMS.

The PTR-ToF instruments introduced by Ionicon Analytik in 2009 had both much higher sensitivities ( $10\text{--}50\text{ cps ppbv}^{-1}$ ) and better mass resolution ( $m/\Delta m \approx 6000$ ) than earlier PTR-ToF instruments ( $< 5\text{ cps ppbv}^{-1}$  and  $m/\Delta m = 100\text{--}1200$ ) (Jordan et al., 2009). The high mass resolution of the ToF analyzer facilitates separation of isobaric isomers (Graus et al., 2010; Sulzer et al., 2014), which enables quantification of more species and reduces possible chemical interferences (Warneke et al., 2015). PTR-ToF instruments have been used successfully in several field campaigns at ground sites to measure concentrations and fluxes of a large suite of VOCs (Müller et al., 2010; Holzinger et al., 2013; Kaser et al., 2013; Park et al., 2013). A PTR-ToF with mass resolution up to  $\sim 1000$  was deployed on the NASA P-

3B research aircraft during the DISCOVER-AQ campaign, demonstrating much higher time resolution and hence better spatial resolution of airborne VOC measurements (Müller et al., 2014a). Recently, a newer version of PTR-ToF equipped with a quadrupole ion guide (PTR-QiToF) was developed and is more sensitive (by a factor of  $\sim 25$ ) than previous version of PTR-ToF using electrostatic ion lens systems (Sulzer et al., 2014). However, detailed characterization (e.g., humidity dependence) and applications of PTR-QiToF instruments to ambient measurements are not currently available in the literature.

In this study, a high-resolution time-of-flight chemical ionization mass spectrometer (ToF-CIMS) utilizing hydronium ions ( $\text{H}_3\text{O}^+$ ) similarly to PTR-MS was developed based on the commercial Aerodyne ToF-CIMS (Lee et al., 2014). This instrument contains two quadrupole ion guides to transport ions from the drift tube reaction region to the time-of-flight mass analyzer. The quadrupole ion guides, as demonstrated in the PTR-QiToF recently (Sulzer et al., 2014), provide better transmission efficiency for the reagent and product ions than the conventional ion lens system. The new instrument was deployed on board the NOAA WP-3D research aircraft during the Shale Oil and Natural Gas Nexus (SONGNEX) campaign in spring of 2015. Here, we will present development and characterization of the instrument and its performance during the SONGNEX campaign.

**Table 1.** Sensitivities and detection limits of  $\text{H}_3\text{O}^+$  ToF-CIMS for various VOC species during the SONGNEX campaign.

VOC species	Ion formula	Sensitivity <sup>1</sup>		Background (cps) <sup>2</sup>	$\alpha$ value <sup>3</sup>	1 s detection limit (ppt)
		ncps/ppb	cps/ppb <sup>2</sup>			
Methanol*	$\text{CH}_4\text{OH}^+$	81	158	128	1.34	397
Acetonitrile*	$\text{C}_2\text{H}_3\text{NH}^+$	376	822	26	1.33	45
Acetaldehyde*	$\text{C}_2\text{H}_4\text{OH}^+$	289	654	499	1.36	195
Acetone*	$\text{C}_3\text{H}_6\text{OH}^+$	354	916	261	1.28	97
Acetic acid	$\text{C}_2\text{H}_4\text{O}_2\text{H}^+$	209	551	660	1.40	283
Furan	$\text{C}_4\text{H}_4\text{OH}^+$	168	470	11	1.26	58
Isoprene*	$\text{C}_5\text{H}_8\text{H}^+$	73	206	26	1.21	162
MVK	$\text{C}_4\text{H}_6\text{OH}^+$	160	454	46	1.24	85
MEK*	$\text{C}_4\text{H}_8\text{OH}^+$	308	886	48	1.21	45
Benzene*	$\text{C}_6\text{H}_6\text{H}^+$	165	493	22	1.48	96
Toluene*	$\text{C}_7\text{H}_8\text{H}^+$	178	579	6	1.39	47
o-Xylene*	$\text{C}_8\text{H}_{10}\text{H}^+$	193	673	4	1.49	40
1,2,4-TMB*	$\text{C}_9\text{H}_{12}\text{H}^+$	185	686	3	1.69	45
$\alpha$ -Pinene	$\text{C}_{10}\text{H}_{16}\text{H}^+$	67	263	2	1.24	67

<sup>1</sup> Sensitivity under dry conditions. <sup>2</sup> Calculations using  $\text{H}_3\text{O}^+$  signal at the typical level of  $2.5 \times 10^6$  cps during the SONGNEX campaign. The signals or sensitivities are not corrected for the ToF duty cycle (see text). <sup>3</sup>  $\alpha$  is the scaling factor of the errors in ion signals relative to Poissonian statistics (Eq. 1). \* Stars indicate that the compounds were calibrated in-flight using the 10-component gas standard.

## 2 $\text{H}_3\text{O}^+$ ToF-CIMS instrument description

A commercial Aerodyne CIMS (Lee et al., 2014) was used to construct the airborne  $\text{H}_3\text{O}^+$  ToF-CIMS (Fig. 1). Briefly, the Aerodyne ToF-CIMS consists of (1) an ion–molecule reaction (IMR) chamber, (2) a small segmented radio frequency (RF)-only quadrupole ion guide that is used as collisional dissociation chamber (SSQ), (3) a second big segmented RF-only quadrupole (BSQ), (4) a series of DC optics that further focus and accelerate the primary beam (PB) and (5) a high-resolution ToF detector (HTOF, Tofwerk AG, Switzerland) (Bertram et al., 2011). In the new  $\text{H}_3\text{O}^+$  ToF-CIMS, the IMR chamber was replaced by a drift tube that is the same as used in PTR-MS (Fig. 1). The drift tube is comprised of stainless steel rings separated by Teflon rings for both vacuum sealing and electronic insulation (de Gouw and Warneke, 2007). A hollow cathode discharge ion source was connected in front of the drift tube to produce high-purity hydronium ions by introducing a flow of  $5 \text{ mL min}^{-1}$  of water vapor. The detailed description for both drift tube and ion source can be found in previous review papers (de Gouw and Warneke, 2007; Blake et al., 2009). In addition to the three-stage split-flow turbo pump (Pfeiffer SplitFlow 310) used for the high vacuum of BSQ, PB and ToF, another turbo pump (Pfeiffer TMH-071-P) was installed to draw air from the SSQ and water vapor from the ion source. A butterfly exhaust throttle valve (MKS T3Bi) was used to control the pumping rate of the newly installed turbo pump (Fig. 1), and the pressure of the SSQ can be adjusted by the opening percentage of the valve. In practice, the pressure of drift tube is also actively controlled (see below) and SSQ pressure only needs to be adjusted sporadically.

The newly built  $\text{H}_3\text{O}^+$  ToF-CIMS was deployed on the NOAA WP-3D aircraft in March–April 2015 as part of the SONGNEX campaign. During SONGNEX, a total of 19 flights were carried out mainly over oil and gas production basins in the western United States. For the detailed flight strategies, the readers are referred to the SONGNEX website ([www.esrl.noaa.gov/csd/projects/songnex](http://www.esrl.noaa.gov/csd/projects/songnex)).

A heated Teflon tube ( $40^\circ\text{C}$ ) mounted inside a winglet on a window plate was used to transport air into the instrument (Fig. S1 in the Supplement). Pressure at the downstream end of the inlet was regulated to 180 mbar using a pressure controller. A PEEK capillary was placed between the pressure controller and drift tube to further reduce the pressure from 180 mbar to the maintained pressure in the drift tube ( $2.40 \pm 0.01$  mbar). During SONGNEX, the 11 cm long drift tube had a drift voltage of 710 V and was heated to  $50^\circ\text{C}$ , which resulted in an  $E/N$  ratio (electric field to number density) of 120 Td ( $1 \text{ Td} = 10^{-17} \text{ V cm}^{-2}$ ) inside the drift tube. The flow of the inlet varied from  $\sim 500 \text{ mL min}^{-1}$  at sea level to  $\sim 100 \text{ mL min}^{-1}$  at 6.5 km of altitude. Background signals of the instrument were determined by passing ambient air for 90 s every 20–40 min through a platinum catalytic converter heated to  $350^\circ\text{C}$ . The catalytic converter was flushed using ambient air continuously for quick switch between ambient and background measurements. In-flight calibrations were performed by adding a small flow ( $0.5\text{--}3.0 \text{ mL min}^{-1}$ ) of a 10-component gas standard (see the list in Table 1) to the inlet flow automatically for 90 s every 1–2 h (Fig. S1). Calibrations were conducted by adding the gas standard flow to clean air from the catalytic converter. Gas standard was also added to ambient air at times when ambient VOC concentrations were stable (e.g., in free troposphere). A diffusion

cell introduced a small amount of 1,3,5-trichlorobenzene ( $C_6H_3Cl_3$ ) into the instrument continuously to facilitate ToF mass calibration at the high ends of the  $m/z$  range. Laboratory experiments show that 1,3,5-trichlorobenzene mainly generates  $C_6H_3Cl_3H^+$  ( $m/z$  180.937, 98.5%) in the instrument, with small contributions from  $C_6H_3Cl_3^+$  ( $m/z$  179.929, 1.0%) and  $C_6H_3Cl_2H^+$  ( $m/z$  145.968, 0.4%). The signals of  $C_6H_3Cl_3H^+$  ion were around 2000 cps during the SONGNEX campaign.

The axial voltage gradients for SSQ and BSQ were tuned using the Thuner software (Tofwerk AG) by maximizing signals of the protonated product ions of several VOC species (acetone, benzene and isoprene), minimizing VOC signals from charge transfer reactions with  $O_2^+$  and maximizing mass resolution of the ToF analyzer before the campaign. In addition, the effects of turning the RF amplitudes of the SSQ and BSQ were explored manually (see below). The voltage of micro-channel plate (MCP) detector for ToF are determined and set before takeoff for each individual flight by maintaining the single ion signal at around  $1.8\text{ mV ns}^{-1}$ , which effectively prevents mass discrimination as the result of MCP aging (Müller et al., 2014b). The extraction frequency of the ToF was set at 25 kHz, which enables the measurement of masses up to  $m/z$  500. During SONGNEX, mass spectra were averaged and stored to 10 Hz and were further averaged afterward to 1 Hz for the analysis shown in this paper.

ToF data were processed using the Tofware software package (v2.5.1) ([www.tofwerk.com/tofware](http://www.tofwerk.com/tofware)) developed by Tofwerk and Aerodyne Research Inc. ([www.aerodyne.com](http://www.aerodyne.com)). The detailed procedures of the ToF data processing have been presented in a previous publication (Stark et al., 2015). Post-measurement mass calibrations were conducted using 6–7 isolated masses, including  $m/z$  19.018 ( $H_3O^+$ ),  $m/z$  29.997 ( $NO^+$ ),  $m/z$  31.989 ( $O_2^+$ ),  $m/z$  37.028 ( $H_3O^+(H_2O)$ ),  $m/z$  55.039 ( $H_3O^+(H_2O)_2$ ),  $m/z$  125.961 ( $FeH_5O_4H^+$ ) and  $m/z$  180.937 ( $C_6H_3Cl_3H^+$ ). Mass calibration of the ToF was accurate within 5–10 ppm for various masses, similar to the results reported for another Aerodyne ToF-CIMS instrument (Lee et al., 2014). Instrument functions (peak shape, peak width and baseline) were derived for each individual flight based on the algorithms shown in Stark et al. (2015). High-resolution peak fitting to the mass spectra was performed using a user-defined peak list with masses up to  $m/z$  181. The typical mass resolution ( $m/\Delta m$ ) for the  $H_3O^+$  ToF-CIMS during the SONGNEX campaign is shown in Fig. S2. The  $m/\Delta m$  in the range of  $m/z$  30–200 (where most VOCs were detected) is 3900–5900 with higher resolution for heavier masses. These mass resolutions are sufficient to separate many isobaric ions (see details in the Supplement and Fig. S3).

In the orthogonal extraction region of the ToF analyzer, ions of different masses have the same energy but different velocities and are therefore extracted at different duty cycles (Chernushevich et al., 2001). The Tofware software corrects

for this effect using the equation of  $I_{\text{corr}} = I_{\text{raw}} \times \sqrt{\frac{55}{m/z}}$  to a reference mass of  $m/z$  55. In this study, all of the signals are reported as the ToF duty cycle corrected signals ( $I_{\text{corr}}$ ), unless otherwise noted.

### 3 $H_3O^+$ ToF-CIMS instrument performance

#### 3.1 Quadrupole ion guides

In addition to hydronium ions ( $H_3O^+$ ), water clusters are also present in the instrument, including protonated water dimers ( $H_3O^+(H_2O)$ ) and protonated water trimers ( $H_3O^+(H_2O)_2$ ). In standard PTR-MS operation, the product ion signals are normalized to the reagent ion count rates to account for drifts in the ion source. Because the reagent ions in the  $H_3O^+$  ToF-CIMS are so strongly dependent on humidity, the measured cluster ion distribution needs to be understood in detail as it affects the normalization procedure and therefore the measured mixing ratios. As the drift tube in  $H_3O^+$  ToF-CIMS is identical to those in PTR-MS, the cluster distribution and their humidity dependence in the drift tube are expected to be similar to PTR-MS, which is understood well and described in detail in de Gouw and Warneke (2007). However, the cluster distribution can be altered in the quadrupole ion guides, because the electric field inside the ion guides is not always the same as that in the drift tube. Thus, the reagent ions and VOC signals as a function of various settings of the quadrupole ion guides are investigated here.

The signals of the reagent ions as a function of the pressure inside the SSQ are shown in Fig. 2. As the SSQ pressure increases from 1.0 to 1.5 mbar, the intensities of all reagent ions increase, indicative of better ion transmission through the SSQ at higher pressures. When the SSQ pressure is higher than 1.5 mbar, the  $H_3O^+$  signal starts to decline slightly and water clusters continue to increase, implying that the reagent ions shift to larger clusters at these SSQ pressures. The ratios of  $H_3O^+(H_2O)/H_3O^+$  ( $R_{37/19}$ ) increase with the SSQ pressure throughout the range studied here. At higher SSQ pressure, the effective de-clustering ability or  $E/N$  ratio is reduced. The  $H_3O^+(H_2O)_2$  ions account for small a fraction of the reagent ions throughout the explored range of SSQ pressures. The signals of protonated benzene and acetone at constant mixing ratios (2.5 ppb) both increase with higher SSQ pressure, although the increase of benzene signals is small when SSQ pressures go beyond 1.5 mbar. The protonated VOC signals correlate better with  $H_3O^+$  than with  $H_3O^+(H_2O)$ , suggesting that  $H_3O^+$  ions are the dominant participant in proton-transfer reactions, even though  $H_3O^+$  ions are measured at comparable levels as  $H_3O^+(H_2O)$  at high SSQ pressures. Along with this observation, the observed slight reduction of  $H_3O^+$  and disproportionately larger enhancement of  $H_3O^+(H_2O)$  with SSQ pressures above 1.5 mbar imply that the transmission of  $H_3O^+$

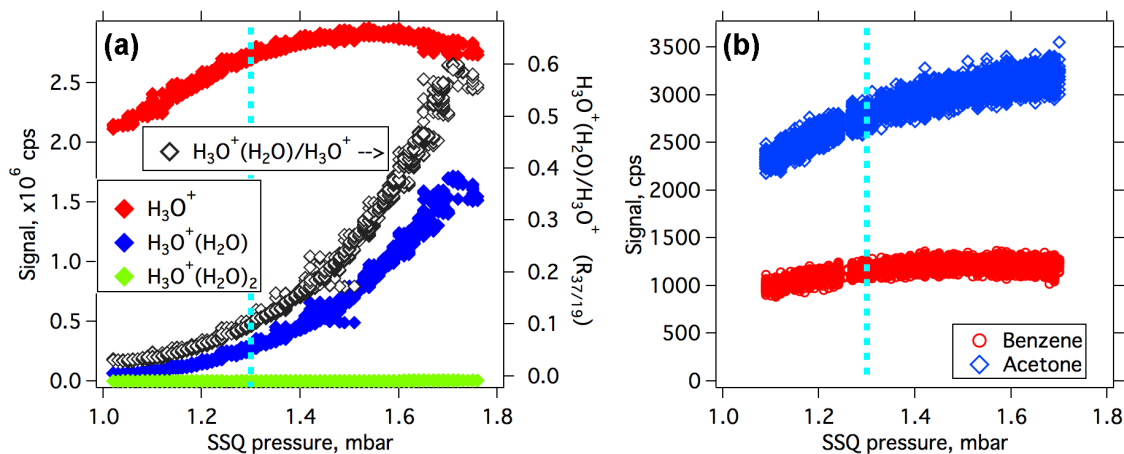


**Figure 2.** (a) Signals of reagent ions and  $\text{H}_3\text{O}^+(\text{H}_2\text{O})/\text{H}_3\text{O}^+$  ratio ( $R_{37/19}$ ) as a function of SSQ pressure. (b) Signals of protonated benzene and acetone at constant mixing ratios of 2.5 ppb as a function of SSQ pressure. The light blue vertical dashed lines indicate the SSQ pressure (1.30 mbar) used during the SONGNEX campaign.

in the SSQ is significantly lower than that of  $\text{H}_3\text{O}^+(\text{H}_2\text{O})$  (and other higher  $m/z$ ). Choosing the optimum SSQ pressure therefore represents a trade-off between higher intensities of the reagent (and VOC) ions and lower signals of water clusters. We have selected to run the instrument with the SSQ pressure at  $1.30 \pm 0.01$  mbar during the SONGNEX campaign.

In addition to the SSQ pressure, the signals of reagent ions and VOC product ions were also explored as a function of RF amplitudes for both SSQ and BSQ (Figs. S4 and S5). From these experiments, the main findings are as follows. (1) As expected, lower RF amplitudes in the BSQ lead to better transmission for light ions but worse ion focusing (Chernushevich et al., 2001). (2) Ion chemistry needs to be taken into account in the SSQ; for example,  $\text{H}_3\text{O}^+$  declines and  $\text{H}_3\text{O}^+(\text{H}_2\text{O})$  increases when RF amplitudes decrease from 80 to 40 V. (3) Variations of VOC signals generally follow the reagent ions, but they are influenced more by poorer focusing at low RF amplitudes, especially for heavier VOC masses. (4)  $\text{O}_2^+$  signals and charge transfer products of aromatics increase quickly when RF amplitudes of the SSQ are higher than 80 V. The high  $\text{O}_2^+$  signals are possibly due to discharge in the SSQ (ToF-CIMS manual indicates that discharge happens with  $>200$  V RF amplitudes), but it warrants further investigation. Continuous increase of  $\text{O}_2^+$  signals with RF amplitudes in BSQ was also observed. To optimize VOC sensitivities and reduce the complexity of mass spectra, the RF amplitudes of the SSQ and BSQ were set to 50 and 350 V, respectively. RF frequencies of SSQ (2.6 MHz, medium mass coil) and BSQ (4.5 MHz, low-mass coil) were set according to manufacturer's suggestions.

### 3.2 Transmission of reagent ions and their humidity dependence

The humidity of the sampled air affects the distribution of the reagent ions in PTR-MS (de Gouw and Warneke, 2007). Figure 3a shows the reagent ion signals vs. water vapor mixing ratios ( $w$ ) of the sampled air from a laboratory experiment. As expected, the  $\text{H}_3\text{O}^+(\text{H}_2\text{O})$  signals increase as the air gets more humidified. The signals of  $\text{H}_3\text{O}^+(\text{H}_2\text{O})_2$  were small but increase quickly with humidity. However, there is also an increase of  $\text{H}_3\text{O}^+$  signals with humidity. Compared to dry air with  $w = 0 \text{ g kg}^{-1}$ , the  $\text{H}_3\text{O}^+$  signals are 52 % higher under the condition with  $w = 22.4 \text{ g kg}^{-1}$  equivalent to a relative humidity (RH) of 90 % at 25 °C. This behavior is in marked contrast to the reported dependence of the reagent ions on humidity in a conventional PTR-MS using ion lenses to transfer ions (de Gouw and Warneke, 2007): in these instruments,  $\text{H}_3\text{O}^+$  decreases and  $\text{H}_3\text{O}^+(\text{H}_2\text{O})$  increases with rising humidity and the total intensities of the two reagent ions are relatively stable with humidity with the remaining difference explainable from the difference in detection efficiency between  $\text{H}_3\text{O}^+$  and  $\text{H}_3\text{O}^+(\text{H}_2\text{O})$ .

The larger  $\text{H}_3\text{O}^+$  signals at higher humidity in the  $\text{H}_3\text{O}^+$  ToF-CIMS are the result of the low transmission efficiency of  $\text{H}_3\text{O}^+$  ions compared to other heavier masses, as demonstrated from the dependence of the reagent ions with SSQ pressures above. The low transmission of  $\text{H}_3\text{O}^+$  ions is related to low-mass cutoff of RF-only quadrupoles (Chernushevich et al., 2001). A reagent ion detected either as  $\text{H}_3\text{O}^+$  or  $\text{H}_3\text{O}^+(\text{H}_2\text{O})$  may undergo many collisions and travel as both  $\text{H}_3\text{O}^+$  and  $\text{H}_3\text{O}^+(\text{H}_2\text{O})$  in the quadrupole ion guides, similarly as shown by previous ion mobility measurement (Warneke et al., 2001). As a result, the transmission efficiency of a reagent ion in the quadrupoles reflects the av-

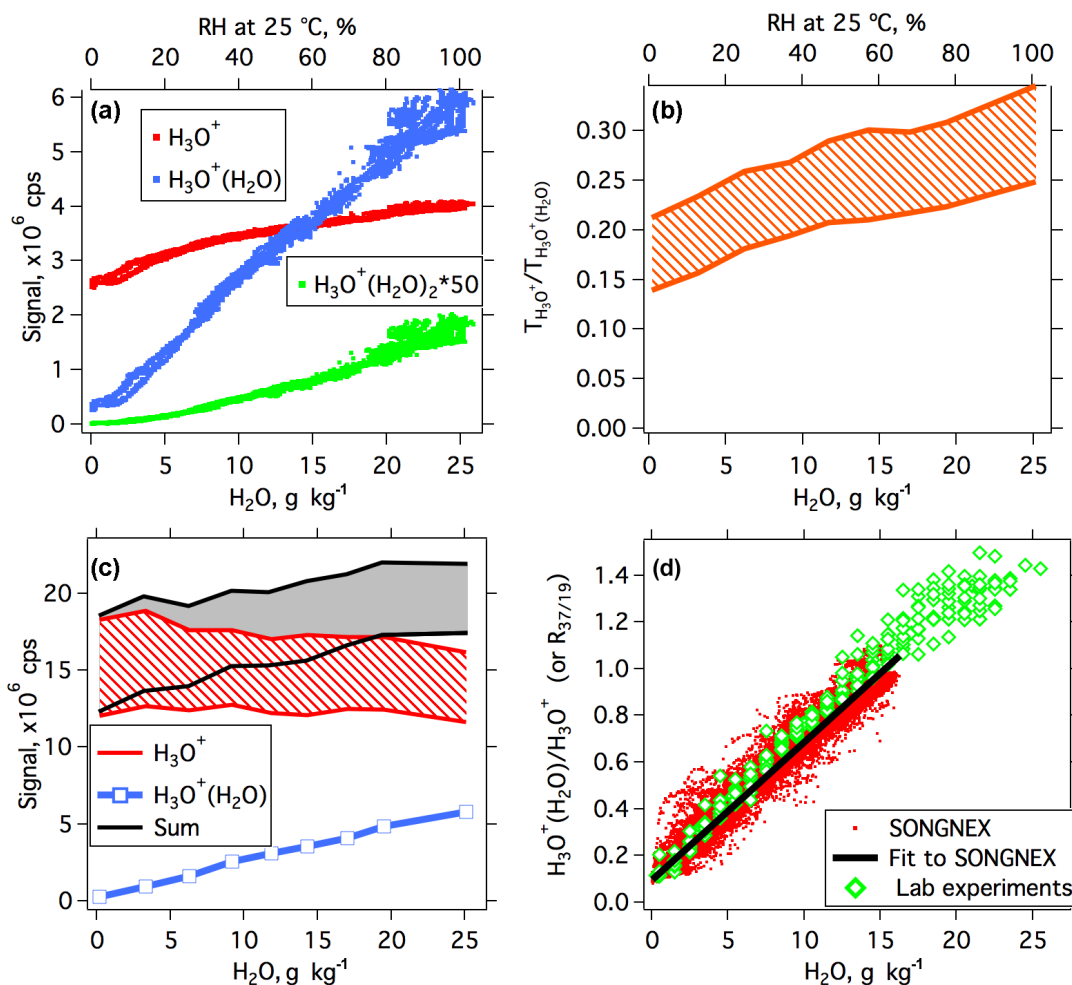


**Figure 3.** (a) Reagent ion signals as a function of water vapor mixing ratios in the instrument. (b) Inferred transmission ratios between  $\text{H}_3\text{O}^+$  and  $\text{H}_3\text{O}^+(\text{H}_2\text{O})$  ions ( $T_{\text{H}_3\text{O}^+}/T_{\text{H}_3\text{O}^+(\text{H}_2\text{O})}$ ) as a function of water vapor mixing ratios. (c) The  $\text{H}_3\text{O}^+$  signals and total signals of the two reagent ions that are corrected to the transmission factor of  $\text{H}_3\text{O}^+(\text{H}_2\text{O})$  ions as a function of water vapor mixing ratios. The measured  $\text{H}_3\text{O}^+(\text{H}_2\text{O})$  signals are also shown. The shaded areas in (b) and (c) indicate the possible ranges of the parameters, which are bounded by estimates from the depletion experiments of methanol and acetonitrile, respectively. (d)  $\text{H}_3\text{O}^+(\text{H}_2\text{O})/\text{H}_3\text{O}^+$  ( $R_{37/19}$ ) as a function of water vapor mixing ratios during SONGNEX and from laboratory experiments. The black line is the linear fit to all of the SONGNEX data.

eraged transmission efficiencies of ions with  $m/z$  19 and  $m/z$  37 weighed by the time the ion spends as  $\text{H}_3\text{O}^+$  vs.  $\text{H}_3\text{O}^+(\text{H}_2\text{O})$ . The strong increase in  $\text{H}_3\text{O}^+$  signal intensity with humidity reflects the fact that while ions may be detected as  $\text{H}_3\text{O}^+$ , they spent a larger fraction of time as  $\text{H}_3\text{O}^+(\text{H}_2\text{O})$  in the SSQ at higher humidity and are therefore transferred with a higher average transmission efficiency.

The transmission efficiency of  $\text{H}_3\text{O}^+$  ions relative to  $\text{H}_3\text{O}^+(\text{H}_2\text{O})$  is quantified using additional laboratory experiments. Methanol and acetonitrile were introduced into the instrument at such high concentrations that significant fractions of the reagent ions were depleted (Fig. S6). Methanol and acetonitrile are used because their product ion masses ( $m/z$  33 and  $m/z$  42) bracket the mass of  $\text{H}_3\text{O}^+(\text{H}_2\text{O})$  ions. We observed more product ions of both methanol ( $\text{CH}_4\text{OH}^+$ ,

$m/z$  33.033) and acetonitrile ( $\text{C}_2\text{H}_3\text{NH}^+$ ,  $m/z$  42.034) than the summed depletion of  $\text{H}_3\text{O}^+$  and  $\text{H}_3\text{O}^+(\text{H}_2\text{O})$ . As the transmission factor of  $\text{H}_3\text{O}^+(\text{H}_2\text{O})$  ions should be in between protonated methanol and acetonitrile ions, the ratios between  $\text{H}_3\text{O}^+$  changes and the changes of the sum of product ions and  $\text{H}_3\text{O}^+(\text{H}_2\text{O})$  ions in each depletion experiment reflect the ratios of the transmission efficiency between  $\text{H}_3\text{O}^+$  and  $\text{H}_3\text{O}^+(\text{H}_2\text{O})$  ( $T_{\text{H}_3\text{O}^+}/T_{\text{H}_3\text{O}^+(\text{H}_2\text{O})}$ ). From the scatterplots in Fig. S6, the  $T_{\text{H}_3\text{O}^+}/T_{\text{H}_3\text{O}^+(\text{H}_2\text{O})}$  ratios are determined to be in the range of 0.21–0.35 and 0.14–0.25 from the experiments with methanol and acetonitrile, respectively (Fig. S7). The discrepancies between the estimates from methanol and acetonitrile may come from the differences between the transmission factors of  $m/z$  33 and  $m/z$  42 (Fig. S8) and/or small amount of methanol–water cluster for

methanol (see Sect. 3.3). The determined  $T_{\text{H}_3\text{O}^+}/T_{\text{H}_3\text{O}^+(\text{H}_2\text{O})}$  ratios are larger at higher water vapor mixing ratios (Figs. 3b and S7), in accordance with the expectation of a higher effective transmission efficiency of  $\text{H}_3\text{O}^+$  ions with increasing humidity discussed above.

The relationship of  $T_{\text{H}_3\text{O}^+}/T_{\text{H}_3\text{O}^+(\text{H}_2\text{O})}$  vs. water vapor mixing ratios shown in Fig. 3b can be used to correct the measured  $\text{H}_3\text{O}^+$  signals to the same transmission efficiency as  $\text{H}_3\text{O}^+(\text{H}_2\text{O})$  (Fig. 3c). The corrected  $\text{H}_3\text{O}^+$  signals exhibit slightly lower signals at higher humidity, which is more similar to the relationship observed in the PTR-MS drift tube (de Gouw and Warneke, 2007). The summed signals of the corrected  $\text{H}_3\text{O}^+$  and measured  $\text{H}_3\text{O}^+(\text{H}_2\text{O})$  are also shown in Fig. 3c. We see higher total reagent ion signals at increasing humidity. It is clear that  $\text{H}_3\text{O}^+$  ions dominate the reagent ions in the drift tube throughout the explored humidity range, even though the measured  $\text{H}_3\text{O}^+$  signals are lower than  $\text{H}_3\text{O}^+(\text{H}_2\text{O})$  ions at high humidity levels. At a high humidity level (RH = 90 % at 25 °C,  $w = 22.4 \text{ g kg}^{-1}$ ),  $\text{H}_3\text{O}^+(\text{H}_2\text{O})$  ions account for 24–30 % of the total reagent ions.

Taken together, both the signals of the reagent ions and their transmission efficiency in the instrument exhibit nonlinear relationships with humidity. The total reagent ion signals can be derived from the determined  $T_{\text{H}_3\text{O}^+}/T_{\text{H}_3\text{O}^+(\text{H}_2\text{O})}$ , but it is associated with significant uncertainties (Fig. 3c). The main goal of the normalization process is to take into account the variations of reagent ions associated with constant humidity (e.g., ion source performance) and the best practice is normalizing to a parameter, which is related to reagent ions and is humidity independent. A simple equation to derive a parameter with little humidity dependence from reagent ion signals seems to be difficult. Thus, the product ion signals will be normalized to  $\text{H}_3\text{O}^+$  signals of  $10^6$  cps to account for drifts in the ion source. Normalization to  $\text{H}_3\text{O}^+$  signals does not involve any mathematical computation of the reagent ions, which may introduce extra uncertainty.

The ratios of  $\text{H}_3\text{O}^+(\text{H}_2\text{O})$  ions to  $\text{H}_3\text{O}^+$  ions ( $R_{37/19}$ ) can be used as a proxy for humidity in PTR-MS (de Gouw et al., 2003a). The dependence of  $R_{37/19}$  with water vapor mixing ratios of the sampled air is shown in Fig. 3d. We see higher  $R_{37/19}$  ratios with increasing humidity from both laboratory experiments and ambient measurements during the SONGNEX, suggesting that  $R_{37/19}$  is also a good internal humidity indicator for the instrument. The agreement between laboratory experiments and ambient data is good, considering that the humidity sensors used for laboratory experiments were not cross-calibrated with the sensors on the NOAA WP-3D. The correlation coefficients from laboratory experiments and SONGNEX ambient data are 0.98 and 0.99, respectively, both indicative of a tight linear relationship of the data points. The intercept in Fig. 3d is the result of excess water vapor entering the drift tube from the ion source. Based on the linear fit to SONGNEX data points in Fig. 3d, the  $R_{37/19}$  ratio in the instrument is 1.4 at a humidity level of

RH = 90 % at 25 °C (or  $w = 22.4 \text{ g kg}^{-1}$ ), which will be used to characterize the instrument response and compare with dry conditions in this study.

### 3.3 The humidity dependence of VOC sensitivities

#### 3.3.1 Species without significant dehydration and hydration

A series of laboratory experiments were performed to describe instrument sensitivities of various VOC species as a function of humidity. Figure 4 shows the results for acetone and toluene from one of the experiments. Constant mixing ratios (8.0 ppb in Fig. 4) of acetone and toluene were introduced into the instruments and the background subtracted raw signals of protonated product ions of the two compounds were observed at various humidities. As described in the previous section,  $R_{37/19}$  is used as the indicator of humidity. Protonated acetone signals increase with rising humidity, whereas protonated toluene signals decline under humidified conditions. The signals of protonated acetone and protonated toluene at the humidity level of  $R_{37/19} = 1.4$ , equivalent to RH = 90 % at 25 °C, are 111 and 57 % of those under dry conditions, respectively. The humidity dependencies of these two species are similar to those for conventional PTR-MS reported in de Gouw and Warneke (2007) (Fig. 4b).

The normalized signals of acetone and toluene from the humidity experiments are shown in Fig. 4c. As illustrated in the previous section,  $\text{H}_3\text{O}^+$  signals are 52 % higher at  $R_{37/19} = 1.4$  relative to dry conditions. The increase of  $\text{H}_3\text{O}^+$  signals with humidity is apparently larger than the increase of protonated acetone, which in turn leads to a reduction of the normalized protonated acetone signals with increasing humidity. Because of the low transmission of  $\text{H}_3\text{O}^+$  ions and clustering/de-clustering effects as described earlier, the normalization to reagent ions leads to a different humidity dependence of the normalized signals in the  $\text{H}_3\text{O}^+$  ToF-CIMS compared to that in the conventional PTR-MS.

The normalized signals at varying humidity levels relative to that at dry conditions for acetone, toluene and other VOC species are determined. After attempts using several different fit functions to describe the data points, a double exponential function was found to achieve the best representation of the data. The fitted humidity curves for acetone, benzene and other VOC species are compiled in Fig. 5. Generally, a stronger humidity dependence was observed for hydrocarbons than for oxygenated VOCs (OVOCs). Comparing the results of the aromatics (benzene, toluene, o-xylene, methylstyrene, 1,2,4-trimethylbenzene and p-cymene), we see less humidity dependence for heavier aromatics. The same trend is also observed for ketones (acetone, MEK, pentanone and hexanone). The heavier species in the two compound series tend to have higher proton affinities (PAs) (Hunter and Lias, 1998), suggesting that proton affinities of the species play a role in the humidity dependence.

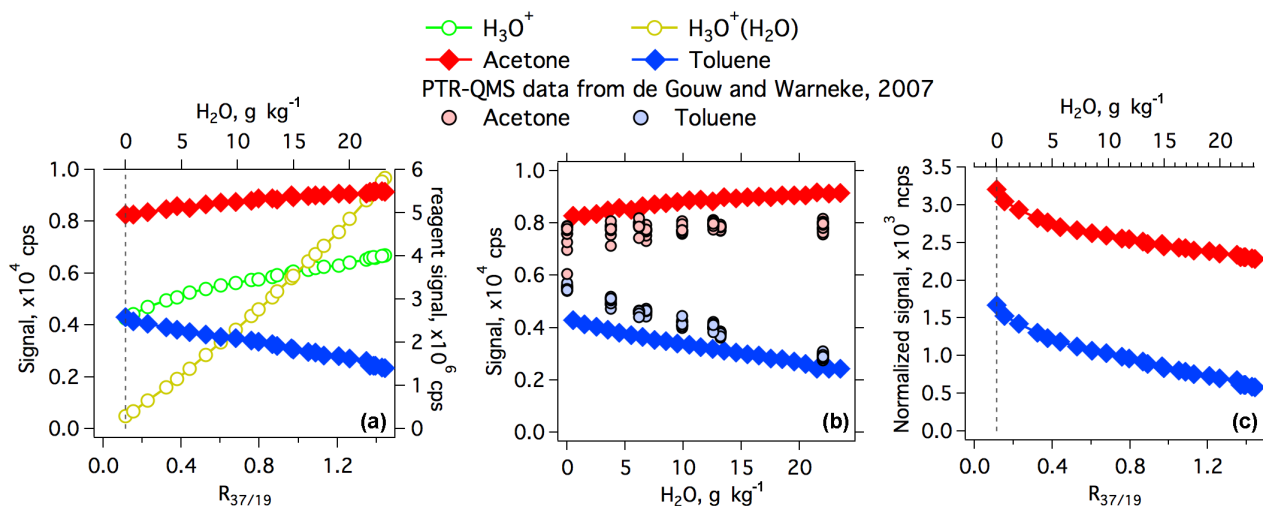


**Figure 4.** Normalization and humidity dependence of acetone and toluene detection from a laboratory experiment. **(a)** Background subtracted raw signals of protonated acetone and toluene with mixing ratios of 8.0 ppb as the function of  $R_{37/19}$ . The signals of  $H_3O^+$  and  $H_3O^+(H_2O)$  are also shown for reference. **(b)** The humidity dependence of raw signals of acetone and toluene compared with the reported humidity dependence of raw signals of the two compounds in a PTR-QMS from Fig. 6b in de Gouw and Warneke (2007). Note that similar signal levels between the two instruments shown in **(b)** are coincident. The relative changes at different humidity levels should be compared. **(c)** Signals of protonated acetone and toluene normalized to the  $H_3O^+$  signal as a function of  $R_{37/19}$ . Vertical dashed line in **(a)** and **(b)** indicated  $R_{37/19}$  under dry conditions.

The fractions of normalized signals at  $R_{37/19} = 1.4$  relative to dry conditions ( $f_{R_{37/19}=1.4}$ ) were determined and plotted as a function of proton affinities of the species in Fig. 5c. A positive correlation between the determined fractions and proton affinities of VOC species is generally observed. This is expected, as a higher proton affinity for a VOC species has several implications: (1) the reaction with  $H_3O^+(H_2O)$  ions is exothermic when the proton affinity exceeds that of water dimer ( $801\text{ kJ mol}^{-1}$ ); and (2) the reaction more readily becomes exothermic through either direct proton transfer or other routes (Midey et al., 2002). The data points in Fig. 5c are color-coded using the permanent dipole moment ( $\mu_D$ ) of the neutrals, which has been shown to affect the efficiency of ligand-switching reactions between VOC species and water clusters (Spanel and Smith, 1995). It is clear that species with  $\mu_D < 1\text{ D}$  are more strongly humidity dependent than the species with  $\mu_D > 1\text{ D}$ , which implies that ligand-switching reactions are important in the instrument as the result of substantial amounts of  $H_3O^+(H_2O)$  ions. Based on proton affinity and permanent dipole moment, the species shown in Fig. 5c can be divided into four groups: group I with  $PA > 801\text{ kJ mol}^{-1}$  and  $\mu_D > 1\text{ D}$  (e.g., acetone); group II with  $PA < 801\text{ kJ mol}^{-1}$  and  $\mu_D > 1\text{ D}$  (e.g., acetaldehyde); group III with  $PA > 801\text{ kJ mol}^{-1}$  and  $\mu_D < 1\text{ D}$  (e.g., isoprene); group IV with  $PA < 801\text{ kJ mol}^{-1}$  and  $\mu_D < 1\text{ D}$  (e.g., benzene). Species in group I (high PA and  $\mu_D$ ) can undergo proton transfer with  $H_3O^+(H_2O)$  and  $H_3O^+$  at similar rate constants, whereas the reactions with  $H_3O^+(H_2O)$  are either not happening or inefficient for species in group IV (low PA

and  $\mu_D$ ). For species in group II (low PA, high  $\mu_D$ ) and III (high PA, low  $\mu_D$ ), ligand-switching and direct proton transfer reactions with  $H_3O^+(H_2O)$  can occur in the instrument, respectively.

The inverse of  $H_3O^+$  signal relative to dry conditions ( $\frac{1}{m_{19}}$ ) was included in Fig. 5 (a and b) as a reference. If the humidity dependence for a VOC species follows this reference line, the raw signal of the VOC actually has no humidity dependence and the lower normalized signals at higher humidity levels are solely the result of normalization to higher  $H_3O^+$  signals. Species above this reference line are associated with higher raw signals at higher humidity, and vice versa. As discussed in Sect. 3.2, the increase of  $H_3O^+$  signals with rising humidity is caused by a higher effective transmission of ions detected as  $H_3O^+$  (Fig. 3b). Thus, the upper limit of the humidity dependence curve should be a flat unity line in Fig. 5 (a and b) (see exceptions in Sect. 3.3.2). Many heavier OVOC masses were observed during SONGNEX, but their humidity dependence was not explored. As higher proton affinities are expected for these heavier OVOC species, the humidity dependence curves for these heavier OVOCs should lie in the shaded area filled by patterns in Fig. 5 (a and b).

### 3.3.2 Species with significant dehydration and hydration

Product ions of the species explored for humidity dependence in the previous section (Sect. 3.3.1) are associated with

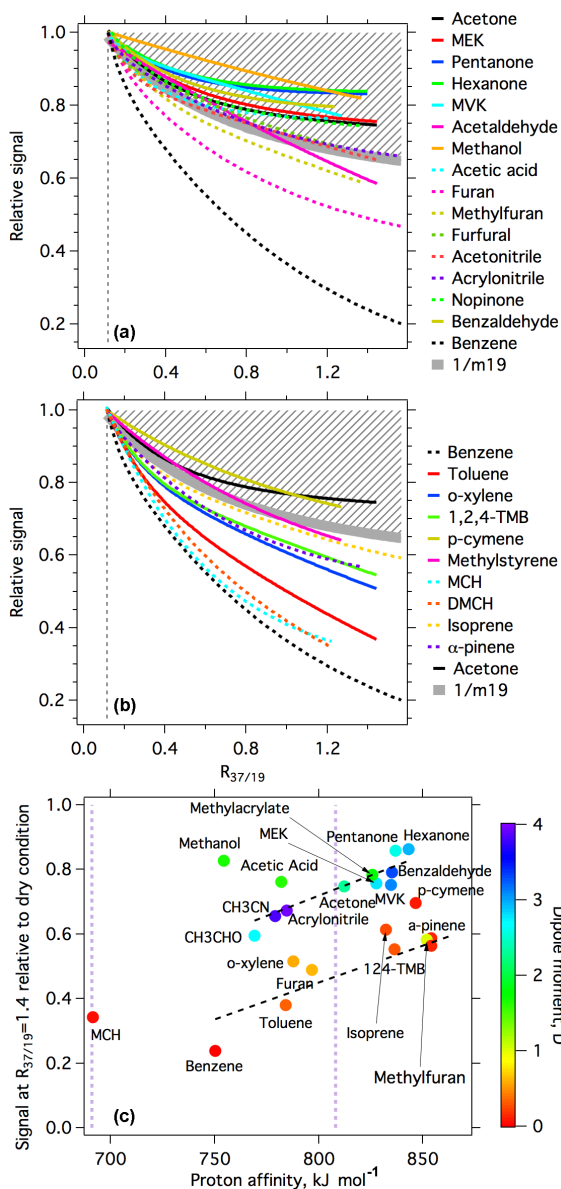


**Figure 5.** Derived humidity dependence curves for the normalized signals relative to dry conditions as a function of  $R_{37/19}$  ratios for oxygenates (a) and hydrocarbons (b), respectively. The humidity-dependent curves of benzene and acetone are shown in both (a) and (b). The thick gray lines indicate the reciprocal of the  $\text{H}_3\text{O}^+$  signal relative to dry conditions ( $\frac{1}{m_{19}}$ ). Vertical dashed lines in (a) and (b) indicate the level of  $R_{37/19}$  under dry conditions. (b) Normalized signals at  $R_{37/19} = 1.4$  (equivalent to RH = 90 % at 25 °C) relative to dry conditions for different VOC species as a function of their proton affinities. Data points are color-coded using the permanent dipole moment of the species. The two purple vertical dashed lines are proton affinities of water and water dimer, respectively. The two black dashed lines indicate the linear fits to the species with permanent dipole moment larger than 1 ( $y = -1.30 + 2.52 \times 10^{-3} \times \text{PA}$ ) and lower than 1 ( $y = -1.38 + 2.29 \times 10^{-3} \times \text{PA}$ ), respectively.

minor dehydration following the proton transfer reaction. Dehydration happens when the product ion of a VOC species fragments by losing one or more water molecules. Propanols and higher alcohols are known to mainly yield dehydration product ions in PTR-MS (Warneke et al., 1996; Spanel and Smith, 1997; Blake et al., 2009). For example, isopropanol ( $\text{C}_3\text{H}_7\text{OH}$ ,  $\text{PA} = 795.4 \text{ kJ mol}^{-1}$ ) is mainly detected as  $\text{C}_3\text{H}_7^+$  ( $m/z$  43.054) rather than  $\text{C}_3\text{H}_8\text{OH}^+$  ( $m/z$  61.065) in  $\text{H}_3\text{O}^+$  ToF-CIMS (Fig. 6a). We see higher  $\text{C}_3\text{H}_8\text{OH}^+/\text{C}_3\text{H}_7^+$  ratios with increasing humidity in the instrument. The measured humidity dependence of  $\text{C}_3\text{H}_7^+$  ions is similar to that of acetaldehyde (and other OVOCs), whereas more  $\text{C}_3\text{H}_8\text{OH}^+$  ions are detected with increasing humidity and the normalized signal of  $\text{C}_3\text{H}_8\text{OH}^+$  ions at  $R_{37/19} = 1.4$  is 1.7 times that of dry air. Similar to i-propanol, a positive dependence of protonated ethanol on humidity is also observed (Fig. 6b), as ethanol fragments significantly by losing a water molecule as well (Baasandorj et al., 2015).

In addition to dehydration, hydrated product ions in the form of  $\text{MH}^+(\text{H}_2\text{O})$  (where  $M$  is the formula of VOC species) are observed, including acetaldehyde, acetone, methanol and acetic acid (Fig. 7a). The ratios of hydration ions to protonated molecular ions ( $\text{MH}^+(\text{H}_2\text{O})/\text{MH}^+$ ) are observed to increase with humidity for these compounds. Among the species investigated, formic acid ( $\text{HCOOH}$ ,  $\text{PA} = 741.8 \text{ kJ mol}^{-1}$ ) and isocyanic acid ( $\text{HNCO}$ ,  $\text{PA} = 720 \text{ kJ mol}^{-1}$ ; Bunkan et al., 2016) are clustering the most, with  $\text{MH}^+(\text{H}_2\text{O})/\text{MH}^+$  ratios of 0.34 and 1.2 at  $R_{37/19} = 1.4$ , respectively. The protonated ions of the two compounds both decrease quickly with humidity, and the normalized signals at  $R_{37/19} = 1.4$  are both only approximately 2 % of those at dry conditions. The signals of hydration ions cannot account for the difference between the humidity-dependent curves of these two compounds and the region other OVOCs occupy in Fig. 5. The reason for the strong humidity dependence of the two compounds is not known, but it is possibly due to enhanced loss of ions after hydration. A similar enhanced loss of ions at higher humidity was observed for formic acid in a PTR-QMS at a low  $E/N$  ratio (85 Td) but not at higher  $E/N$  ratios (Baasandorj et al., 2015). Baasandorj et al. (2015) (see Fig. 5f in their paper) showed that, at the low  $E/N$  ratio (85 Td), protonated ions of formic acid decrease by 12 ncps ppb<sup>-1</sup> and hydration ions only increase by 6 ncps ppb<sup>-1</sup> going from RH = 18 to 88 %. The enhanced loss of isocyanic acid at higher humidity might be related to its hydrolysis, which is reported to be accelerated by water dimer and trimer (Raspoe et al., 1998).

The examples of isopropanol, formic acid and isocyanic acid suggest that the humidity dependence can be affected by dehydration and hydration processes of the product ions. The abundance of water molecules affects the equilibrium ratios of the respective ion pairs. In contrast, there are some species associated with significant fragmentation without the water molecule as a neutral product, e.g., monoterpenes and p-cymene, which exhibit similar humidity dependence as other

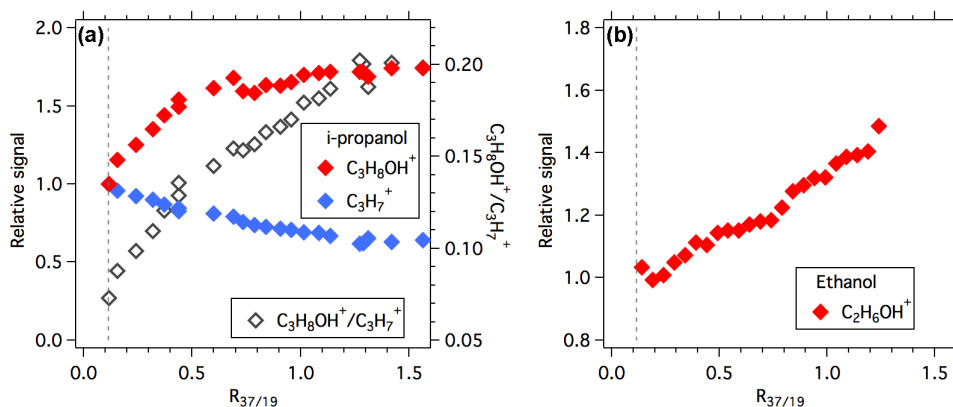


**Figure 6.** (a) Normalized signals relative to dry conditions for protonated and dehydrated ions of isopropanol as a function of  $R_{37/19}$  ratios. The vertical dashed line indicates the level of  $R_{37/19}$  under dry conditions. (b) Normalized signals relative to dry conditions for protonated ion of ethanol as a function of  $R_{37/19}$  ratios.

VOCs (Fig. 5c). Therefore, special attention should be paid to the humidity dependence of the species associated with either significant fragmentation by losing water molecule or significant molecule–water clusters.

### 3.4 Background correction, in-flight calibration and detection limits

The humidity dependence curves illustrated in Fig. 5 were used to correct the normalized signals of various VOC species from measurements made during SONGNEX. After that, background signals were averaged for each measurement cycle and interpolated to the periods between background measurements. Two features in ambient measurements were considered in the interpolation of background signals. First, we observed continuously decrease of background signals for some ions during the flights (Fig. S9b). The decrease of background signals cannot be avoided during aircraft measurements, as the instrument only had 2–3 h start-up time in the morning of each flight day and the instrument backgrounds usually become lower as the instrument runs. Second, background signals for many ions are dependent on humidity in the air, even after the correction for the humidity dependence of their sensitivities (Fig. S9d). This is also of particular importance for aircraft measurements, as a rapid change of humidity is encountered during aircraft ascents and descents (de Gouw and Warneke, 2007). Exponential decay function was used to describe the continuous decline of background signals, whereas humidity dependence of background signals was described using linear relationships with one of the humidity indicators ( $R_{37/19}$ ,  $\text{H}_3\text{O}^+(\text{H}_2\text{O})_2/\text{H}_3\text{O}^+$ ,  $\text{O}_2^+$  signals and  $\text{CO}_2^+$  signals). Both effects were important for some ions and they were taken into account by consecutive implementation of the procedures (Fig. S9c). For other ions, a simple linear interpolation was adopted (Fig. S9e). The variations of instrument

backgrounds with instrument running time and humidity may also be critical for other PTR-MS and CIMS instruments, especially for aircraft deployments and in some circumstances when meteorological conditions change quickly during ground measurements. The procedures shown here should be easy to incorporate into these measurements when necessary.

The measurements of each in-flight calibration are averaged in the same way as the background measurements. The results for benzene, isoprene, acetaldehyde and acetone during the SONGNEX campaign are shown in Fig. 8. Each of the four species represents one of the four groups of compounds described in Sect. 3.3. The calibration results for the four species show tight linear correlations between corrected normalized signals and calculated mixing ratios from the gas standard ( $R > 0.995$ ), indicating stable instrument performance from flight to flight during the SONGNEX campaign. No clear dependence of sensitivities on  $R_{37/19}$  is observed, demonstrating that the effects of humidity on the sensitivities are properly accounted for by the procedures described above. The measured sensitivities for various VOC species are shown in Table 1, which lists sensitivities under dry conditions. The sensitivities for most VOC species of interest are better than  $400 \text{ cps ppb}^{-1}$ , with several species higher than  $800 \text{ cps ppb}^{-1}$ . The lower sensitivity for methanol is consistent with previous studies (Warneke et al., 2015), whereas lower sensitivities for isoprene and  $\alpha$ -pinene are due to the fragmentation of their product ions.

The counting statistics of the ions follow a Poisson distribution, i.e., the  $1\sigma$  error of counting  $N$  ions is  $\sqrt{N}$ . Recent studies showed that the high-resolution peak fitting to the ToF mass spectra can add significant additional noise to the fitted peak intensities of the masses (Corbin et al., 2015; Cubison and Jimenez, 2015). Figure 9 shows standard deviations of the background signals vs. the background signals themselves from the individual zeroing periods for the

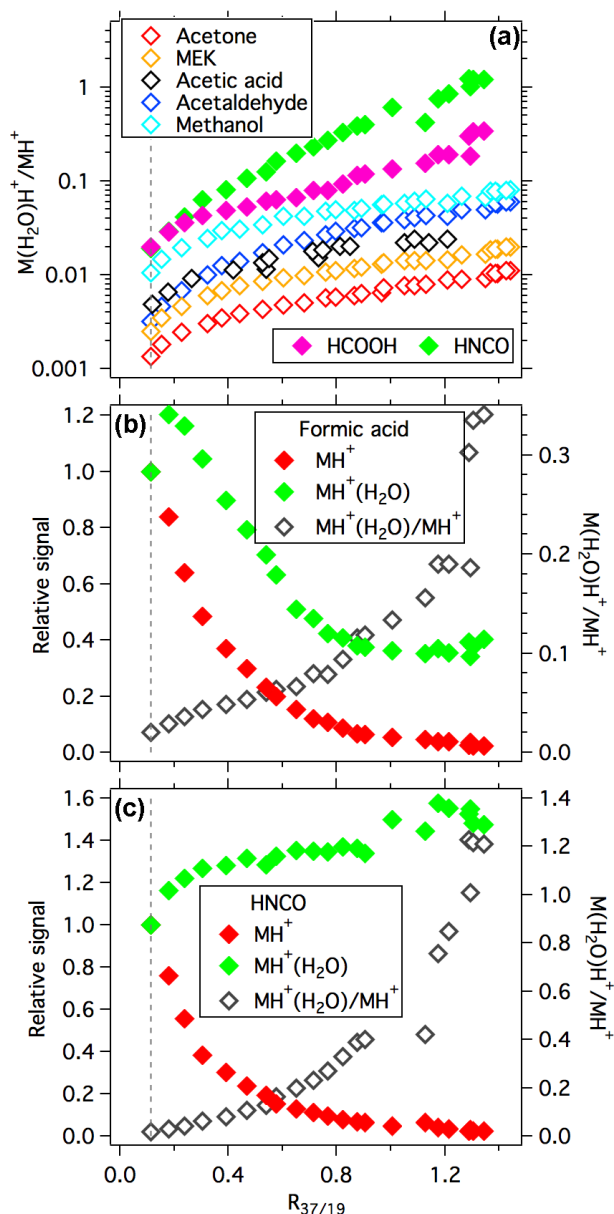


**Figure 7.** (a) The ratios of hydrated ions to protonated ions for several OVOC species as a function of  $R_{37/19}$  ratios. (b) and (c) Normalized signals relative to dry conditions for protonated and hydrated ions of formic acid (HCOOH, b) and isocyanic acid (HNCO, c) as a function of  $R_{37/19}$  ratios. The ratios of hydrated ions to protonated ions for formic acid and isocyanic acid vs.  $R_{37/19}$  ratios are also shown in (b) and (c), respectively. Vertical dashed lines in each panel indicate the level of  $R_{37/19}$  under dry conditions.

masses listed in Table 1 during one SONGNEX flight (27 April 2015). Note that the signals shown in Fig. 9 were not corrected for the ToF duty cycle, so they represent the actual ion signals detected by the MCP. Real variations of background signals due to instrument drift may contribute some to the standard deviations of background signals. Thus, data

points in Fig. 9 are best viewed as the upper limits of the errors from counting statistics. Most of the data are observed in the region between  $\sqrt{N}$  and  $2 \times \sqrt{N}$ , suggesting that high-resolution peak fitting can increase the errors in the ion signals by as much as a factor of 2 for the VOC masses in Table 1.

The signal-to-noise ratio ( $S/N$ ) of the species  $X$  from a CIMS instrument can be expressed by (Bertram et al., 2011)

$$\frac{S}{N} = \frac{C_f [X] t}{\alpha \times \sqrt{C_f [X] t + 2Bt}} \quad (1)$$

Here,  $[X]$  is the mixing ratio of the species (ppb),  $C_f$  is the sensitivity of the species ( $\text{cps ppb}^{-1}$ ) and  $B$  is the background count (cps), both of which are values without corrections for the ToF duty cycle.  $t$  is the sampling time (s).  $\alpha$  is the scaling factor of the errors in ion signals relative to Poissonian statistics and is used to account for the additional errors from high-resolution peak fitting.  $\alpha$  for each species is determined from Fig. 9 (see Table 1 for values). We define the detection limit as the mixing ratio with a  $S/N$  ratio of 3. The calculated 1 s detection limits for various species are listed in Table 1. The 1 s detection limits are better than 100 ppt for most species. Higher detection limits for acetaldehyde, acetic acid, isoprene, methanol and ethanol are the result of higher background counts for the former two species and lower sensitivities for the latter three species, respectively.

Figure 10 compares sensitivities and detection limits of methanol, acetone and benzene between the NOAA PTR-QMS from several previous campaigns (Warneke et al., 2011) and the new  $\text{H}_3\text{O}^+$  ToF-CIMS during SONGNEX. As discussed in Warneke et al. (2011), the performance of the NOAA PTR-QMS improved gradually as a result of many instrumental developments, which led to higher sensitivities and lower detection limits. The results of PTR-QMS also suggest the variability in sensitivity of a single instrument due to small changes in electronics tuning and hardware configurations. As shown in Fig. 10, the sensitivity of acetone in the new  $\text{H}_3\text{O}^+$  ToF-CIMS is similar to that of PTR-QMS in the recent campaigns (CalNex and UBWOS 2013), whereas sensitivities of methanol and acetone are somewhat lower than the PTR-QMS. The performance of a commercial PTR-ToF (PTR-TOF 8000, Ionicon Analytik) during the UBWOS 2013 (Warneke et al., 2015) is also included in Fig. 10. We observed much higher sensitivities for our  $\text{H}_3\text{O}^+$  ToF-CIMS than the PTR-ToF used in UBWOS 2013. The large difference in the sensitivities between the PTR-ToF and  $\text{H}_3\text{O}^+$  ToF-CIMS is mainly attributed to the difference between ion lenses used in the PTR-ToF to transfer ions from the drift tube to the mass analyzer and the quadrupole ion guides used in  $\text{H}_3\text{O}^+$  ToF-CIMS. A large enhancement in sensitivities of a PTR-ToF by using quadrupole ion guides was recently also demonstrated in a PTR-QiToF instrument from Ionicon Analytik (Sulzer et al., 2014), which achieved a benzene sensitivity up to  $2900 \text{ cps ppb}^{-1}$ . The total counts measured in each 15 s period (the typical cycle time for

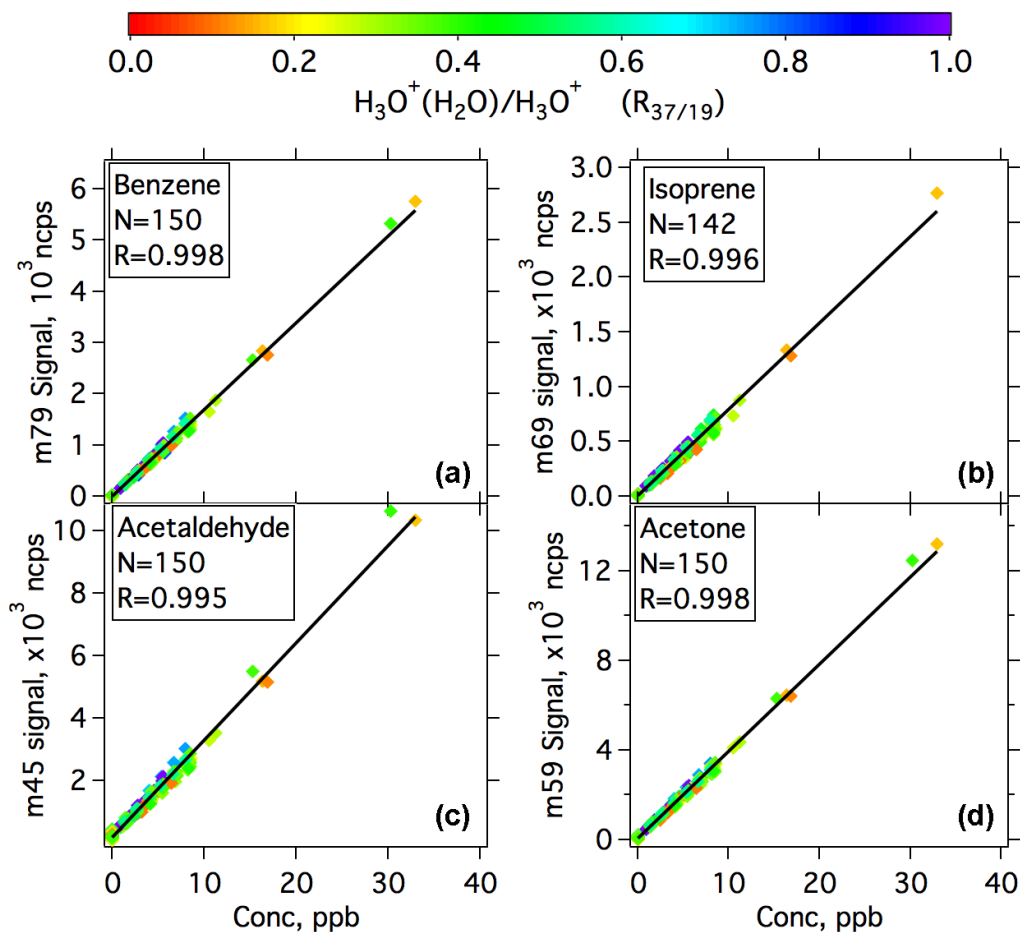


**Figure 8.** In-flight calibration results of benzene (a), isoprene (b), acetaldehyde (c) and acetone (d) during the SONGNEX campaign. Signals for the species have been humidity corrected. Data points are color-coded using  $R_{37/19}$  ratios. The total times ( $N$ ) when gas standard was introduced into the instrument during SONGNEX and correlation coefficients ( $R$ ) are shown in the text box.

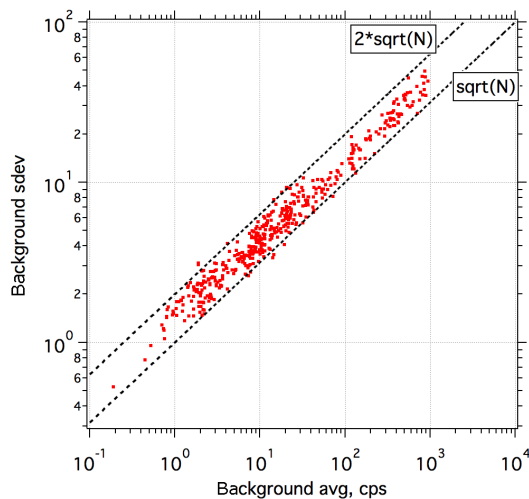


**Figure 9.** Scatterplot of the standard deviations of background signals vs. the measured background signals from a flight on 27 April 2015 during SONGNEX. In this graph, the signals are not corrected for the ToF duty cycle to better reflect the counting statistics of the ToF detector. The two dashed lines are  $\sqrt{N}$  and  $2 \times \sqrt{N}$ .

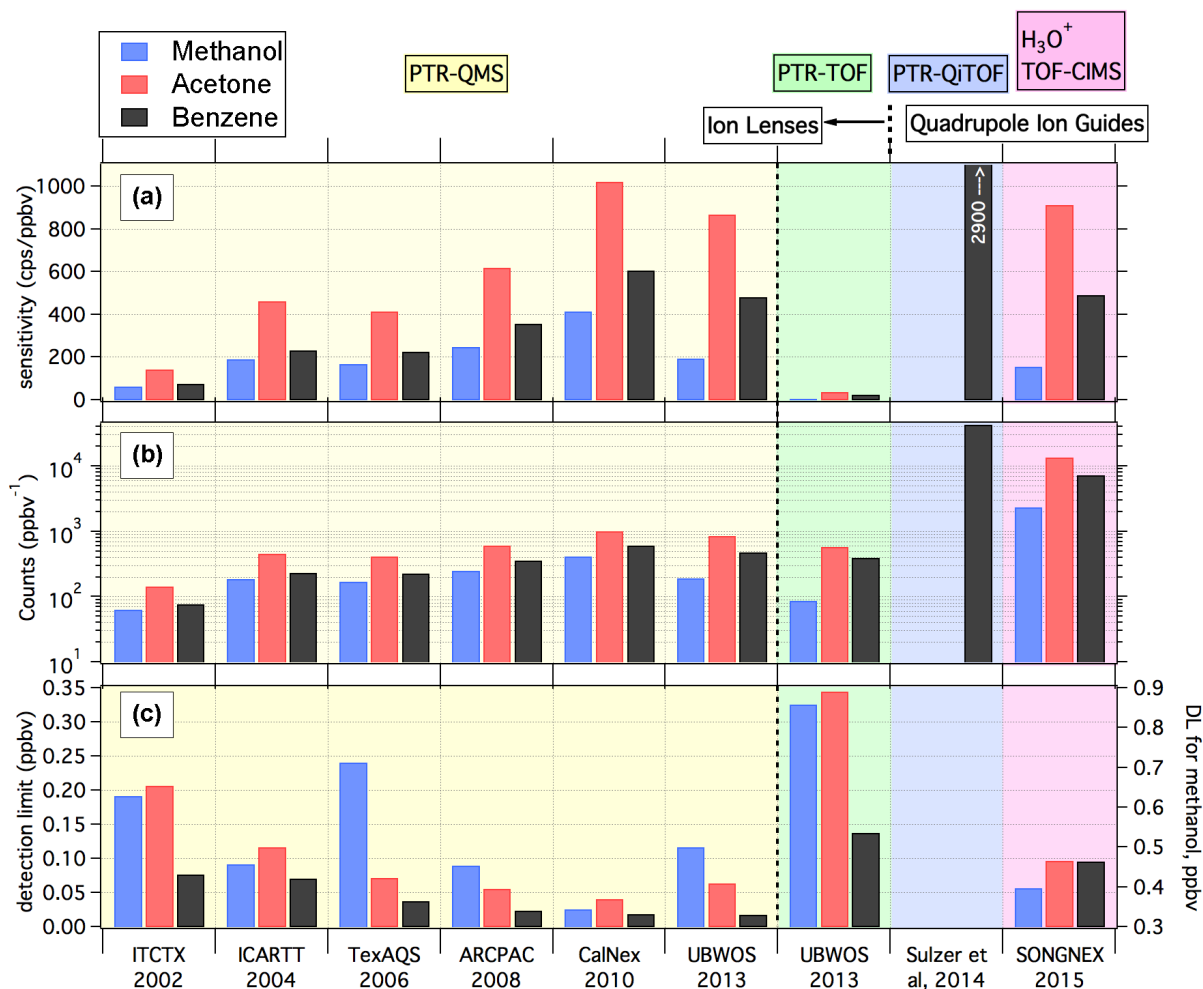


**Figure 10.** Comparison of the sensitivities (a), total ion counts from measurements in a period of 15 s (b) and 1 s detection limits (c) of methanol, acetone and benzene for the NOAA PTR-QMS (Warneke et al., 2011), a PTR-ToF during UBWOS 2013 (Warneke et al., 2015), the PTR-QiToF in Sulzer et al. (2014) and the H<sub>3</sub>O<sup>+</sup> ToF-CIMS presented here during SONGNEX. In (b), we assume that the PTR-QMS was operated at the typical cycle length of 15 s with 1 s dwell time for the three compounds as have been the norm during our aircraft measurements. Note that the detection limits (DL) of methanol in (c) are drawn on the right axis.

PTR-QMS) are calculated and shown in the middle panel in Fig. 10. In terms of total counts in 15 s period, the overall signal to noise of the ToF instruments compares very favorably to the PTR-QMS.

Consistent with the sensitivities, 1 s detection limits of H<sub>3</sub>O<sup>+</sup> ToF-CIMS are close to those in PTR-QMS and better than those of the PTR-ToF used during the UBWOS 2013. As with sensitivities, the detection limits of ToF instruments compare more favorably to QMS when measured data are averaged to the total cycle length of a PTR-QMS to scan the selected masses for their dwell time. We note that the detection limits for methanol, acetone and benzene in the PTR-QiToF were not reported in Sulzer et al. (2014), and hence a comparison with H<sub>3</sub>O<sup>+</sup> ToF-CIMS is not possible at this point.

### 3.5 Intercomparisons with gas chromatography–mass spectrometry (GC-MS)

In addition to H<sub>3</sub>O<sup>+</sup> ToF-CIMS for VOC measurements, whole air samples were collected into canisters in-flight and were analyzed post-flight by GC-MS (iWAS) during the SONGNEX campaign. A total of 72 samples were obtained for most flights. The fill time for each canister was 3–15 s depending on aircraft altitude. A brief description of the iWAS system was provided in recent publications (de Gouw et al., 2015; Warneke et al., 2016). A few compounds were measured by both H<sub>3</sub>O<sup>+</sup> ToF-CIMS and the iWAS system, including benzene, toluene and C8 aromatics. For C8 aromatics, the H<sub>3</sub>O<sup>+</sup> ToF-CIMS measured the total mixing ratios of the isomers, whereas the iWAS system was able to mea-

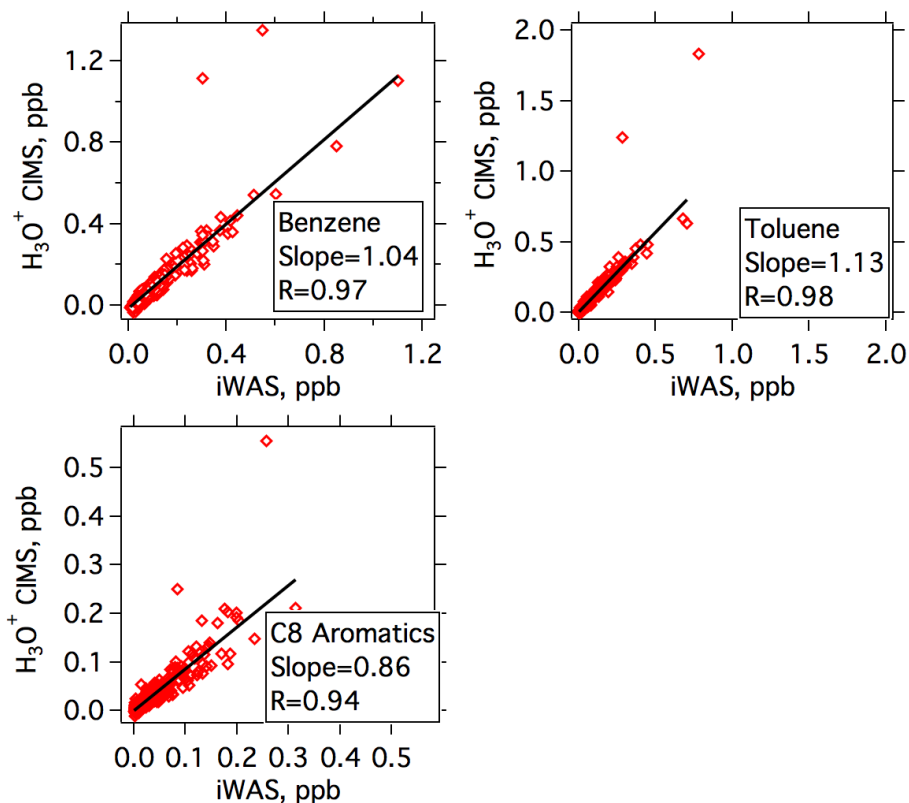


**Figure 11.** Comparison of measured mixing ratios of benzene, toluene and C8 aromatics between the  $\text{H}_3\text{O}^+$  ToF-CIMS and iWAS (Lerner et al., 2016) during the SONGNEX campaign.

sure mixing ratios for the individual isomers (o-xylene, m/p-xylene and ethylbenzene).

Figure 11 compares measured results for benzene, toluene and C8 aromatics between  $\text{H}_3\text{O}^+$  ToF-CIMS and iWAS. The agreement between the two instruments is good for all three aromatic species, with slopes in the range of 0.89–1.1 and correlation coefficients ( $R$ ) larger than 0.9. We note that there are a few data points with larger disagreement, which are the result of imperfect time alignment of the two measurements during large transient concentration spikes downwind from point sources.

### 3.6 Applications to ambient measurements

As mentioned above, the  $\text{H}_3\text{O}^+$  ToF-CIMS was deployed on board the NOAA WP-3D during the SONGNEX campaign. Figure 12 shows measurement results from a portion of a flight on 13 April 2015 over the Denver–Julesburg Basin, which is an active oil and gas extraction region. Mixing ratios of benzene and toluene were elevated over and downwind from the oil/gas field. Several concentration spikes of the two aromatics were observed and attributed to large point sources related to oil and gas activities. Urban emissions may also contribute to the mixing ratios of benzene and toluene, when the NOAA WP-3D flew over the cities (Loveland, Fort

Collins and Greeley) in the area. As shown in Fig. 12, variations of benzene and toluene mixing ratios below 100 ppt still tracked each other well, illustrating the low detection limits of the two compounds in the  $\text{H}_3\text{O}^+$  ToF-CIMS. As the emissions of aromatics and other VOCs from motor vehicles are declining in both US and European cities (Warneke et al., 2012; Derwent et al., 2014), the need for techniques (e.g., our  $\text{H}_3\text{O}^+$  ToF-CIMS) that can measure these compounds rapidly and accurately with low detection limits is increasing.

Concentration peaks of acetonitrile were detected several times in this period, when the aircraft sampled plumes from agricultural burns in the area (de Gouw et al., 2003b). The concentration peaks of acetonitrile were pretty narrow, especially the one at 21:34 UTC (see the inserted graph in Fig. 12b). These small fire plumes could easily have been missed if a PTR-QMS had been applied for the detection of acetonitrile, as PTR-QMS has a duty cycle of only a few percent for each individual mass, as shown in the inserted plot in Fig. 12b. Along with acetonitrile, furan and furfural were also observed in these biomass burning plumes. Furan is a known emission from biomass burning and has been detected in the atmosphere mainly using PTR-MS (de Gouw and Warneke, 2007; Karl et al., 2007). In PTR-QMS, furan

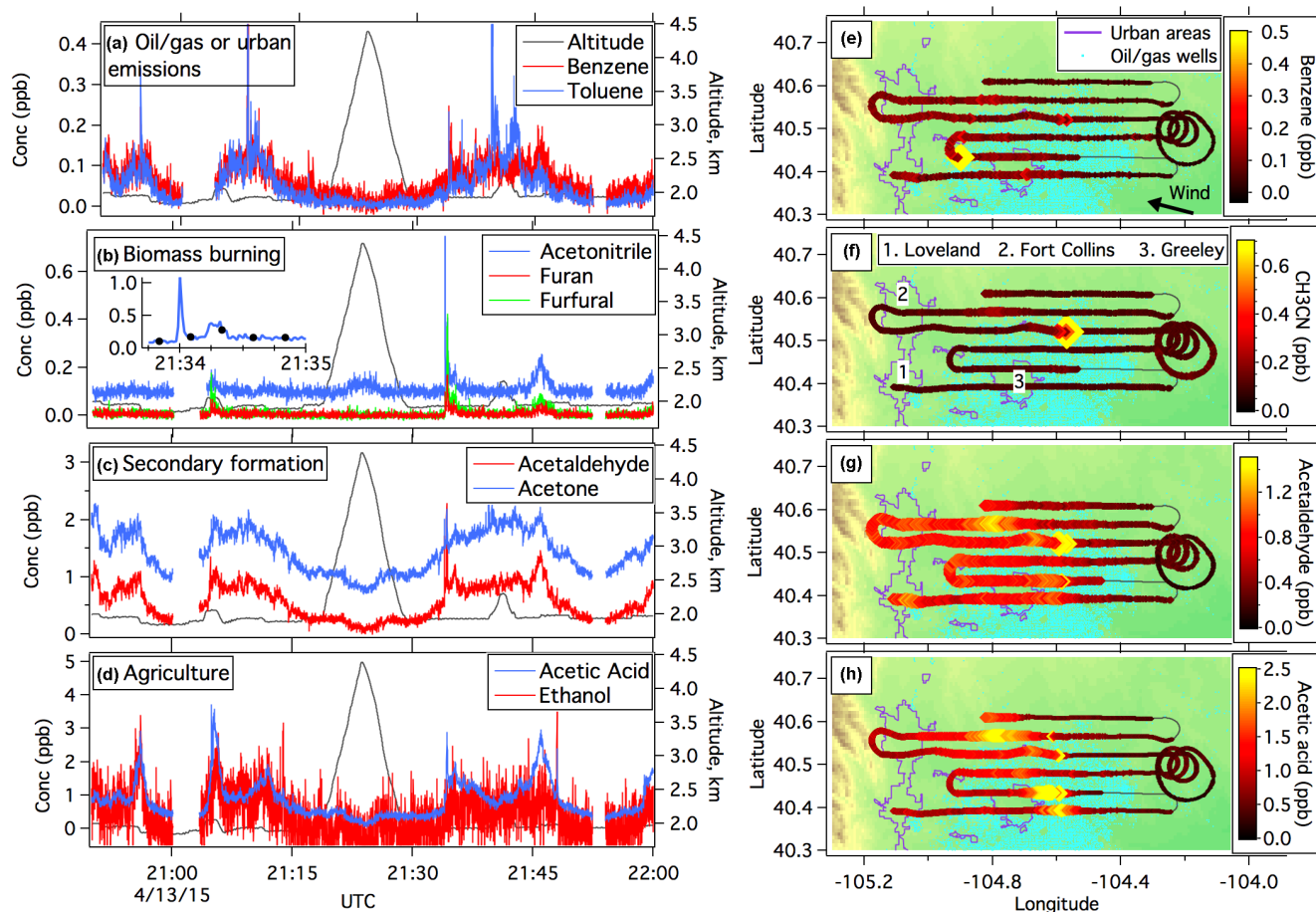


**Figure 12.** VOC measurements by the  $\text{H}_3\text{O}^+$  ToF-CIMS for the characterization of air masses and atmospheric photochemistry during a part of the flight (20:50–22:00 UTC) on 13 April 2015 over the Denver–Julesburg basin. Time series of various VOC species from oil/gas or urban emissions (a), biomass burning (b), secondary formation (c) and agricultural emissions (d) are shown. The inserted plot in (b) highlights acetonitrile around 21:34 UTC, where the black dots indicate re-sampled acetonitrile data every 15 s, reflecting measurement results had a PTR–QMS been deployed on board the NOAA WP-3D. Flight tracks color-coded using mixing ratios of benzene (e), acetonitrile (f), acetaldehyde (g) and acetic acid (h) are shown in the right panels. Urban regions and locations of oil and gas wells are indicated in the right panels. The arrow in (e) indicates wind direction in the boundary layer during this period.

cannot be distinguished from isoprene. Its aldehyde derivatives, furfurals, were only measured in a recent laboratory experiment of biomass burning emissions (Stockwell et al., 2015) and in a forest fire plume in the USA (Müller et al., 2016), both by PTR-ToF.

The third class of compounds shown in Fig. 12 is acetaldehyde and acetone. Time series of the two OVOCs were similar to those of benzene and toluene with elevated mixing ratios over and downwind from the oil and gas wells, but they lacked the concentration spikes observed for the aromatics, consistent with secondary formation as their main sources. Acetaldehyde and acetone were also enhanced in the biomass burning plumes.

As a final example, acetic acid and ethanol were observed in both oil/gas and biomass burning plumes. Additional peaks of acetic acid and ethanol were detected shortly

before and after 21:00 UTC. These enhanced mixing ratios were believed to be the result of emissions from agricultural facilities in this area. Weld County, the main flight area shown in Fig. 12, is home to over half a million beef and dairy cattle in over 100 feedlot facilities. Emissions of acetic acid and ethanol from dairy operations have been reported recently in the Central Valley of California (Gentner et al., 2014).

Figure 12 demonstrates that four different groups of VOC species exhibited with distinctly different time series and spatial distributions as a result of their different sources. The examples in Fig. 12 illustrate that the high-time-resolution data set from  $\text{H}_3\text{O}^+$  ToF-CIMS provides important information on characterizations of various air masses in the atmosphere. Along with unique tracers (e.g., acetonitrile for biomass burning), rich information on the chemical signa-

tures will help to identify and separate the contributions of different sources to air mass components in the atmosphere. Measurements of secondary products, in conjunction with primary emissions will be valuable to constrain chemical evolution of gas-phase organic carbon in the atmosphere.

#### 4 Conclusions

In this study, an aircraft-deployable  $\text{H}_3\text{O}^+$  ToF-CIMS instrument was developed based on a commercial Aerodyne ToF-CIMS. We characterize the humidity dependence of reagent ions and instrument sensitivities for various VOC species. The new  $\text{H}_3\text{O}^+$  ToF-CIMS has sensitivities in the range of 100–1000 cps ppbv<sup>-1</sup> for many VOCs of interest and the 1 s detection limits are in the range of 20–500 ppt, depending on product ion masses and their instrument backgrounds. The instrument was deployed on board the NOAA WP-3D research aircraft as part of the SONGNEX campaign in March–April of 2015. The measured mixing ratios for several aromatics from the  $\text{H}_3\text{O}^+$  ToF-CIMS agreed very well with independent GC measurements from whole air samples. Some initial results from the instrument demonstrate that the  $\text{H}_3\text{O}^+$  ToF-CIMS data set will be extremely valuable for the characterization of VOC emissions and photochemistry in the atmosphere.

We showed that the low transmission of  $\text{H}_3\text{O}^+$  ions as a result of low-mass cutoff of RF-only quadrupoles and secondary ion chemistry inside the quadrupole ion guides lead to the unusual humidity dependence of reagent ions. This issue complicates signal normalization and interpretation of the humidity dependence of VOC sensitivities. Further development by removal of the SSQ may ameliorate this issue and is being considered. We also anticipate a further increase in sensitivities from these modifications, as shown in a recent publication (Sulzer et al., 2014). We show that many instrument settings, including SSQ pressure, RF amplitudes in quadrupoles and the axial voltage gradients along the quadrupoles, affect both reagent ions and significantly in our instrument. We also note that transmission efficiency of  $\text{H}_3\text{O}^+$  ions may be compromised when tuning for best VOC sensitivities. Thus, the low transmission of  $\text{H}_3\text{O}^+$  ions may be heavily influenced by various settings of the quadrupole ion guides. It is unknown whether the next generation of PTR-MS (i.e., PTR-QiToF) that uses quadrupole ion guides for ion transmission is affected by the similar low-mass cutoff problem and secondary ion chemistry in the quadrupole ion guide. Instruments using different ion chemistry are expected to behave differently with these settings. Therefore, characterization of each individual instrument for these variations and calibrations using authentic standards is essential for generating high-quality measurement data with these sophisticated CIMS instruments.

**The Supplement related to this article is available online at doi:10.5194/amt-9-2735-2016-supplement.**

*Acknowledgements.* We would like to thank Andy Newman for providing the permeation source of formic acid and Yong Liu and James Roberts for providing the calibration source of isocyanic acid. A. Koss acknowledges support from the NSF Graduate Fellowship Program and the CIRES Graduate Student Research Award. We gratefully acknowledge the support from our colleagues at the NOAA Aircraft Operations Center for help with the installation of the instrument on the NOAA WP-3D and conducting the flights.

Edited by: E. C. Apel

#### References

- Atkinson, R.: Atmospheric chemistry of VOCs and  $\text{NO}_x$ , *Atmospheric Environment*, 34, 2063–2101, 2000.
- Baasandorj, M., Millet, D. B., Hu, L., Mitroo, D., and Williams, B. J.: Measuring acetic and formic acid by proton-transfer-reaction mass spectrometry: sensitivity, humidity dependence, and quantifying interferences, *Atmos. Meas. Tech.*, 8, 1303–1321, doi:10.5194/amt-8-1303-2015, 2015.
- Bertram, T. H., Kimmel, J. R., Crisp, T. A., Ryder, O. S., Yatavelli, R. L. N., Thornton, J. A., Cubison, M. J., Gonin, M., and Worsnop, D. R.: A field-deployable, chemical ionization time-of-flight mass spectrometer, *Atmos. Meas. Tech.*, 4, 1471–1479, doi:10.5194/amt-4-1471-2011, 2011.
- Blake, R. S., Whyte, C., Hughes, C. O., Ellis, A. M., and Monks, P. S.: Demonstration of proton-transfer reaction time-of-flight mass spectrometry for real-time analysis of trace volatile organic compounds, *Anal. Chem.*, 76, 3841–3845, doi:10.1021/ac0498260, 2004.
- Blake, R. S., Monks, P. S., and Ellis, A. M.: Proton-Transfer Reaction Mass Spectrometry, *Chem. Rev.*, 109, 861–896, doi:10.1021/Cr800364q, 2009.
- Bunkan, A. J., Mikoviny, T., Nielsen, C.J., Wisthaler, A., and Zhu, L.: Experimental and Theoretical Study of the OH-Initiated Photo-oxidation of Formamide, *J. Phys. Chem. A*, 120, 1222–1230, doi:10.1021/acs.jpca.6b00032, 2016.
- Chernushevich, I. V., Loboda, A. V., and Thomson, B. A.: An introduction to quadrupole-time-of-flight mass spectrometry, *J. Mass Spectrom.*, 36, 849–865, doi:10.1002/jms.207, 2001.
- Corbin, J. C., Othman, A., Allan, J. D., Worsnop, D. R., Haskins, J. D., Sierau, B., Lohmann, U., and Mensah, A. A.: Peak-fitting and integration imprecision in the Aerodyne aerosol mass spectrometer: effects of mass accuracy on location-constrained fits, *Atmos. Meas. Tech.*, 8, 4615–4636, doi:10.5194/amt-8-4615-2015, 2015.
- Cubison, M. J. and Jimenez, J. L.: Statistical precision of the intensities retrieved from constrained fitting of overlapping peaks in high-resolution mass spectra, *Atmos. Meas. Tech.*, 8, 2333–2345, doi:10.5194/amt-8-2333-2015, 2015.

- de Gouw, J. and Warneke, C.: Measurements of volatile organic compounds in the earth's atmosphere using proton-transfer-reaction mass spectrometry, *Mass Spectrom. Rev.*, 26, 223–257, 2007.
- de Gouw, J. A., Goldan, P. D., Warneke, C., Kuster, W. C., Roberts, J. M., Marchewka, M., Bertman, S. B., Pszenny, A. A. P., and Keene, W. C.: Validation of proton transfer reaction-mass spectrometry (PTR-MS) measurements of gas-phase organic compounds in the atmosphere during the New England Air Quality Study (NEAQS) in 2002, *J. Geophys. Res.-Atmos.*, 108, 4682, doi:10.1029/2003JD003863, 2003a.
- de Gouw, J. A., Warneke, C., Parrish, D. D., Holloway, J. S., Trainer, M., and Fehsenfeld, F. C.: Emission sources and ocean uptake of acetonitrile (CH<sub>3</sub>CN) in the atmosphere, *J. Geophys. Res.-Atmos.*, 108, 4329, doi:10.1029/2002JD002897, 2003b.
- de Gouw, J. A., McKeen, S. A., Aikin, K. C., Brock, C. A., Brown, S. S., Gilman, J. B., Graus, M., Hanisco, T., Holloway, J. S., Kaiser, J., Keutsch, F. N., Lerner, B. M., Liao, J., Markovic, M. Z., Middlebrook, A. M., Min, K. E., Neuman, J. A., Nowak, J. B., Peischl, J., Pollack, I. B., Roberts, J. M., Ryerson, T. B., Trainer, M., Veres, P. R., Warneke, C., Welti, A., and Wolfe, G. M.: Airborne measurements of the atmospheric emissions from a fuel ethanol refinery, *J. Geophys. Res.-Atmos.*, 120, 4385–4397, doi:10.1002/2015jd023138, 2015.
- Derwent, R. G., Dorn, J. I. R., Dollard, G. J., Dumitrean, P., Mitchell, R. F., Murrells, T. P., Telling, S. P., and Field, R. A.: Twenty years of continuous high time resolution volatile organic compound monitoring in the United Kingdom from 1993 to 2012, *Atmos. Environ.*, 99, 239–247, doi:10.1016/j.atmosenv.2014.10.001, 2014.
- Ennis, C. J., Reynolds, J. C., Keely, B. J., and Carpenter, L. J.: A hollow cathode proton transfer reaction time of flight mass spectrometer, *Int. J. Mass Spectrom.*, 247, 72–80, doi:10.1016/j.ijms.2005.09.008, 2005.
- Gentner, D. R., Ford, T. B., Guha, A., Boulanger, K., Brioude, J., Angevine, W. M., de Gouw, J. A., Warneke, C., Gilman, J. B., Ryerson, T. B., Peischl, J., Meinardi, S., Blake, D. R., Atlas, E., Lonneman, W. A., Kleindienst, T. E., Beaver, M. R., Clair, J. M. St., Wennberg, P. O., VandenBoer, T. C., Markovic, M. Z., Murphy, J. G., Harley, R. A., and Goldstein, A. H.: Emissions of organic carbon and methane from petroleum and dairy operations in California's San Joaquin Valley, *Atmos. Chem. Phys.*, 14, 4955–4978, doi:10.5194/acp-14-4955-2014, 2014.
- Graus, M., Muller, M., and Hansel, A.: High Resolution PTR-TOF: Quantification and Formula Confirmation of VOC in Real Time, *J. Am. Soc. Mass Spectrom.*, 21, 1037–1044, doi:10.1016/j.jasms.2010.02.006, 2010.
- Hallquist, M., Wenger, J. C., Baltensperger, U., Rudich, Y., Simpson, D., Claeys, M., Dommen, J., Donahue, N. M., George, C., Goldstein, A. H., Hamilton, J. F., Herrmann, H., Hoffmann, T., Iinuma, Y., Jang, M., Jenkin, M. E., Jimenez, J. L., Kiendler-Scharr, A., Maenhaut, W., McFiggans, G., Mentel, Th. F., Monod, A., Prévôt, A. S. H., Seinfeld, J. H., Surratt, J. D., Szmigielski, R., and Wildt, J.: The formation, properties and impact of secondary organic aerosol: current and emerging issues, *Atmos. Chem. Phys.*, 9, 5155–5236, doi:10.5194/acp-9-5155-2009, 2009.
- Holzinger, R., Goldstein, A. H., Hayes, P. L., Jimenez, J. L., and Timkovsky, J.: Chemical evolution of organic aerosol in Los Angeles during the CalNex 2010 study, *Atmos. Chem. Phys.*, 13, 10125–10141, doi:10.5194/acp-13-10125-2013, 2013.
- Hunter, E. P. L. and Lias, S. G.: Evaluated Gas Phase Basicities and Proton Affinities of Molecules: An Update, *J. Phys. Chem. Ref. Data*, 27, 413–656, doi:10.1063/1.556018, 1998.
- Isaksen, I. S. A., Granier, C., Myhre, G., Berntsen, T. K., Dal-søren, S. B., Gauss, M., Klimont, Z., Benestad, R., Bousquet, P., Collins, W., Cox, T., Eyring, V., Fowler, D., Fuzzi, S., Jöckel, P., Laj, P., Lohmann, U., Maione, M., Monks, P., Prevot, A. S. H., Raes, F., Richter, A., Rognerud, B., Schulz, M., Shindell, D., Stevenson, D. S., Storelvmo, T., Wang, W. C., van Weele, M., Wild, M., and Wuebbles, D.: Atmospheric composition change: Climate-Chemistry interactions, *Atmos. Environ.*, 43, 5138–5192, doi:10.1016/j.atmosenv.2009.08.003, 2009.
- Jordan, A., Haidacher, S., Hanel, G., Hartungen, E., Mark, L., Seehauser, H., Schottkowsky, R., Sulzer, P., and Mark, T. D.: A high resolution and high sensitivity proton-transfer-reaction time-of-flight mass spectrometer (PTR-TOF-MS), *Int. J. Mass Spectrom.*, 286, 122–128, doi:10.1016/j.ijms.2009.07.005, 2009.
- Karl, T. G., Christian, T. J., Yokelson, R. J., Artaxo, P., Hao, W. M., and Guenther, A.: The Tropical Forest and Fire Emissions Experiment: method evaluation of volatile organic compound emissions measured by PTR-MS, FTIR, and GC from tropical biomass burning, *Atmos. Chem. Phys.*, 7, 5883–5897, doi:10.5194/acp-7-5883-2007, 2007.
- Kaser, L., Karl, T., Schnitzhofer, R., Graus, M., Herdinger-Blatt, I. S., DiGangi, J. P., Sive, B., Turnipseed, A., Hornbrook, R. S., Zheng, W., Flocke, F. M., Guenther, A., Keutsch, F. N., Apel, E., and Hansel, A.: Comparison of different real time VOC measurement techniques in a ponderosa pine forest, *Atmos. Chem. Phys.*, 13, 2893–2906, doi:10.5194/acp-13-2893-2013, 2013.
- Lee, B. H., Lopez-Hilfiker, F. D., Mohr, C., Kurten, T., Worsnop, D. R., and Thornton, J. A.: An iodide-adduct high-resolution time-of-flight chemical-ionization mass spectrometer: application to atmospheric inorganic and organic compounds, *Environ. Sci. Technol.*, 48, 6309–6317, doi:10.1021/es500362a, 2014.
- Lerner, B., Gilman, J., Aikin, K., Atlas, E., Goldan, P., Graus, M., Hendershot, R., Isaacman-VanWertz, G., Koss, A., Kuster, W., Lueb, R., McLaughlin, R., Peischl, J., Sueper, D., Ryerson, T., Tokarek, T., Warneke, C., Yuan, B., and Gouw, J. D.: An Improved, Automated Whole-Air Sampler and Gas Chromatography Mass Spectrometry Analysis System for Volatile Organic Compounds in the Atmosphere, *Atmos. Meas. Tech. Discuss.*, submitted, 2016.
- Lindinger, W., Hansel, A., and Jordan, A.: On-line monitoring of volatile organic compounds at pptv levels by means of proton-transfer-reaction mass spectrometry (PTR-MS) – Medical applications, food control and environmental research, *Int. J. Mass Spectro.*, 173, 191–241, 1998.
- Midey, A. J., Williams, S., Arnold, S. T., and Viggiano, A. A.: Reactions of H<sub>3</sub>O<sup>+</sup>(H<sub>2</sub>O)<sub>0,1</sub> with Alkylbenzenes from 298 to 1200 K, *J. Phys. Chem. A*, 106, 11726–11738, doi:10.1021/jp014141e, 2002.
- Mielke, L. H., Erickson, D. E., McLuckey, S. A., Muller, M., Wisthaler, A., Hansel, A., and Shepson, P. B.: Development of a Proton-Transfer Reaction-Linear Ion Trap Mass Spectrometer for Quantitative Determination of Volatile Organic Compounds, *Anal. Chem.*, 80, 8171–8177, doi:10.1021/ac801328d, 2008.

- Müller, M., Graus, M., Ruuskanen, T. M., Schnitzhofer, R., Bamberger, I., Kaser, L., Titzmann, T., Hörtnagl, L., Wohlfahrt, G., Karl, T., and Hansel, A.: First eddy covariance flux measurements by PTR-TOF, *Atmos. Meas. Tech.*, 3, 387–395, doi:10.5194/amt-3-387-2010, 2010.
- Müller, M., Mikoviny, T., Feil, S., Haidacher, S., Hanel, G., Hartungen, E., Jordan, A., Märk, L., Mutschlechner, P., Schotchkowsky, R., Sulzer, P., Crawford, J. H., and Wisthaler, A.: A compact PTR-ToF-MS instrument for airborne measurements of volatile organic compounds at high spatiotemporal resolution, *Atmos. Meas. Tech.*, 7, 3763–3772, doi:10.5194/amt-7-3763-2014, 2014a.
- Müller, M., Mikoviny, T., and Wisthaler, A.: Detector aging induced mass discrimination and non-linearity effects in PTR-ToF-MS, *Int. J. Mass Spectrom.*, 365–366, 93–97, doi:10.1016/j.ijms.2013.12.008, 2014b.
- Müller, M., Anderson, B. E., Beyersdorf, A. J., Crawford, J. H., Diskin, G. S., Eichler, P., Fried, A., Keutsch, F. N., Mikoviny, T., Thornhill, K. L., Walega, J. G., Weinheimer, A. J., Yang, M., Yokelson, R. J., and Wisthaler, A.: In situ measurements and modeling of reactive trace gases in a small biomass burning plume, *Atmos. Chem. Phys.*, 16, 3813–3824, doi:10.5194/acp-16-3813-2016, 2016.
- Park, J.-H., Goldstein, A. H., Timkovsky, J., Fares, S., Weber, R., Karlik, J., and Holzinger, R.: Active Atmosphere-Ecosystem Exchange of the Vast Majority of Detected Volatile Organic Compounds, *Science*, 341, 643–647, doi:10.1126/science.1235053, 2013.
- Raspoet, G., Nguyen, M. T., McGarraghy, M., and Hegarty, A. F.: Experimental and Theoretical Evidence for a Concerted Catalysis by Water Clusters in the Hydrolysis of Isocyanates, *J. Org. Chem.*, 63, 6867–6877, doi:10.1021/jo98063+, 1998.
- Spanel, P. and Smith, D.: Reactions of Hydrated Hydronium Ions and Hydrated Hydroxide Ions with Some Hydrocarbons and Oxygen-Bearing Organic Molecules, *J. Phys. Chem.*, 99, 15551–15556, doi:10.1021/j100042a033, 1995.
- Spanel, P. and Smith, D.: SIFT studies of the reactions of  $\text{H}_3\text{O}^+$ ,  $\text{NO}^+$  and  $\text{O}_2^+$  with a series of alcohols, *Int. J. Mass Spectrom.*, 167, 375–388, 1997.
- Stark, H., Yatayelli, R. L. N., Thompson, S. L., Kimmel, J. R., Cubison, M. J., Chhabra, P. S., Canagaratna, M. R., Jayne, J. T., Worsnop, D. R., and Jimenez, J. L.: Methods to extract molecular and bulk chemical information from series of complex mass spectra with limited mass resolution, *Int. J. Mass Spectrom.*, 389, 26–38, doi:10.1016/j.ijms.2015.08.011, 2015.
- Steeghs, M. M. L., Sikkens, C., Crespo, E., Cristescu, S. M., and Harren, F. J. M.: Development of a proton-transfer reaction ion trap mass spectrometer: Online detection and analysis of volatile organic compounds, *Int. J. Mass Spectrom.*, 262, 16–24, doi:10.1016/j.ijms.2006.09.031, 2007.
- Stockwell, C. E., Veres, P. R., Williams, J., and Yokelson, R. J.: Characterization of biomass burning emissions from cooking fires, peat, crop residue, and other fuels with high-resolution proton-transfer-reaction time-of-flight mass spectrometry, *Atmos. Chem. Phys.*, 15, 845–865, doi:10.5194/acp-15-845-2015, 2015.
- Sulzer, P., Hartungen, E., Hanel, G., Feil, S., Winkler, K., Mutschlechner, P., Haidacher, S., Schotchkowsky, R., Gansch, D., Seehauser, H., Striednig, M., Jürschik, S., Breiev, K., Lanza, M., Herbig, J., Märk, L., Märk, T. D., and Jordan, A.: A Proton Transfer Reaction-Quadrupole interface Time-Of-Flight Mass Spectrometer (PTR-QiTOF): High speed due to extreme sensitivity, *Int. J. Mass Spectrom.*, 368, 1–5, doi:10.1016/j.ijms.2014.05.004, 2014.
- Tanimoto, H., Aoki, N., Inomata, S., Hirokawa, J., and Sadanaga, Y.: Development of a PTR-TOFMS instrument for real-time measurements of volatile organic compounds in air, *Int. J. Mass Spectrom.*, 263, 1–11, doi:10.1016/j.ijms.2007.01.009, 2007.
- Warneke, C., Kuczynski, J., Hansel, A., Jordan, A., Vogel, W., and Lindinger, W.: Proton transfer reaction mass spectrometry (PTR-MS): propanol in human breath, *Int. J. Mass Spectrom.*, 154, 61–70, doi:10.1016/0168-1176(96)04369-8, 1996.
- Warneke, C., van der Veen, C., Luxembourg, S., de Gouw, J. A., and Kok, A.: Measurements of benzene and toluene in ambient air using proton-transfer-reaction mass spectrometry: calibration, humidity dependence, and field intercomparison, *Int. J. Mass Spectrom.*, 207, 167–182, 2001.
- Warneke, C., Kato, S., De Gouw, J. A., Goldan, P. D., Kuster, W. C., Shao, M., Lovejoy, E. R., Fall, R., and Fehsenfeld, F. C.: Online volatile organic compound measurements using a newly developed proton-transfer ion-trap mass spectrometry instrument during New England Air Quality Study – Intercontinental Transport and Chemical Transformation 2004: Performance, intercomparison, and compound identification, *Environ. Sci. Technol.*, 39, 5390–5397, doi:10.1021/es050602o, 2005.
- Warneke, C., Veres, P., Holloway, J. S., Stutz, J., Tsai, C., Alvarez, S., Rappenglueck, B., Fehsenfeld, F. C., Graus, M., Gilman, J. B., and de Gouw, J. A.: Airborne formaldehyde measurements using PTR-MS: calibration, humidity dependence, intercomparison and initial results, *Atmos. Meas. Tech.*, 4, 2345–2358, doi:10.5194/amt-4-2345-2011, 2011.
- Warneke, C., de Gouw, J. A., Holloway, J. S., Peischl, J., Ryerson, T. B., Atlas, E., Blake, D., Trainer, M., and Parrish, D. D.: Multiyear trends in volatile organic compounds in Los Angeles, California: Five decades of decreasing emissions, *J. Geophys. Res.*, 117, D00V17, doi:10.1029/2012jd017899, 2012.
- Warneke, C., Veres, P., Murphy, S. M., Soltis, J., Field, R. A., Graus, M. G., Koss, A., Li, S.-M., Li, R., Yuan, B., Roberts, J. M., and de Gouw, J. A.: PTR-QMS versus PTR-TOF comparison in a region with oil and natural gas extraction industry in the Uintah Basin in 2013, *Atmos. Meas. Tech.*, 8, 411–420, doi:10.5194/amt-8-411-2015, 2015.
- Warneke, C., Trainer, M., de Gouw, J. A., Parrish, D. D., Fahey, D. W., Ravishankara, A. R., Middlebrook, A. M., Brock, C. A., Roberts, J. M., Brown, S. S., Neuman, J. A., Lerner, B. M., Lack, D., Law, D., Huebler, G., Pollack, I., Sjostedt, S., Ryerson, T. B., Gilman, J. B., Liao, J., Holloway, J., Peischl, J., Nowak, J. B., Aikin, K., Min, K.-E., Washenfelder, R. A., Graus, M. G., Richardson, M., Markovic, M. Z., Wagner, N. L., Welti, A., Veres, P. R., Edwards, P., Schwarz, J. P., Gordon, T., Dube, W. P., McKeen, S., Brioude, J., Ahmadov, R., Bougiatioti, A., Lin, J., Nenes, A., Wolfe, G. M., Hanesco, T. F., Lee, B. H., Lopez-Hilfiker, F. D., Thornton, J. A., Keutsch, F. N., Kaiser, J., Mao, J., and Hatch, C.: Instrumentation and Measurement Strategy for the NOAA SENEX Aircraft Campaign as Part of the Southeast Atmosphere Study 2013, *Atmos. Meas. Tech. Discuss.*, doi:10.5194/amt-2015-388, in review, 2016.